

AD-A260 621



2

# NAVAL POSTGRADUATE SCHOOL Monterey, California



**S** DTIC  
ELECTE  
FEB 23 1993 **D**  
**E**

## THESIS

Spectra of Stable Sonoluminescence

by

Stephen D. Lewia

December, 1992

Thesis Advisor:

Xavier K. Maruyama  
Anthony A. Atchley

Approved for public release; distribution is unlimited

93-03752



1992



REPORT DOCUMENTATION PAGE			
1a. REPORT SECURITY CLASSIFICATION UNCLASSIFIED		1b. RESTRICTIVE MARKINGS	
2a. SECURITY CLASSIFICATION AUTHORITY		3. DISTRIBUTION/AVAILABILITY OF REPORT Approved for public release; distribution is unlimited.	
2b. DECLASSIFICATION/DOWNGRADING SCHEDULE			
4. PERFORMING ORGANIZATION REPORT NUMBER(S)		5. MONITORING ORGANIZATION REPORT NUMBER(S)	
6a. NAME OF PERFORMING ORGANIZATION Naval Postgraduate School	6b. OFFICE SYMBOL (if applicable) Code 33	7a. NAME OF MONITORING ORGANIZATION Naval Postgraduate School	
6c. ADDRESS (City, State, and ZIP Code) Monterey, CA 93943-5000		7b. ADDRESS (City, State, and ZIP Code) Monterey, CA 93943-5000	
8a. NAME OF FUNDING/SPONSORING ORGANIZATION	8b. OFFICE SYMBOL (if applicable)	9. PROCUREMENT INSTRUMENT IDENTIFICATION NUMBER	
8c. ADDRESS (City, State, and ZIP Code)		10. SOURCE OF FUNDING NUMBERS	
		Program Element No	Project No
		Task No	Work Unit Accession Number
11. TITLE (Include Security Classification) SPECTRA OF STABLE SONOLUMINESCENCE			
12. PERSONAL AUTHOR(S) Lewis, Stephen Douglas			
13a. TYPE OF REPORT Master's Thesis	13b. TIME COVERED From To	14. DATE OF REPORT (year, month, day) December 1992	15. PAGE COUNT 94
16. SUPPLEMENTARY NOTATION The views expressed in this thesis are those of the author and do not reflect the official policy or position of the Department of Defense or the U.S. Government.			
17. COSATI CODES		18. SUBJECT TERMS (continue on reverse if necessary and identify by block number)	
FIELD	GROUP	Sonoluminescence Spectrum	
19. ABSTRACT (continue on reverse if necessary and identify by block number) The continuous emission of picosecond pulses of light has been observed to originate from a bubble trapped at the pressure antinode of a resonant sound field in water and in water/glycerin mixtures. The spectra of this light in several solutions has been measured with a scanning monochromator/photomultiplier detector system. The spectra are broadband and show strong emission in the UV region. A comparison of this measurement to two other independently produced spectra is made. The spectra are also modeled by a blackbody radiation distribution to determine an effective blackbody temperature and a size is deduced as if sonoluminescence were characterized by blackbody radiation.			
20. DISTRIBUTION/AVAILABILITY OF ABSTRACT <input checked="" type="checkbox"/> UNCLASSIFIED/UNLIMITED <input type="checkbox"/> SAME AS REPORT <input type="checkbox"/> DTIC USERS		21. ABSTRACT SECURITY CLASSIFICATION UNCLASSIFIED	
22a. NAME OF RESPONSIBLE INDIVIDUAL Xavier K. Maruyama		22b. TELEPHONE (Include Area code) (408)-646-2431	22c. OFFICE SYMBOL PH-MX

Approved for public release; distribution is unlimited.

Spectra of Stable Sonoluminescence

by

Stephen D. Lewia  
Lieutenant, United States Navy  
B.S., United States Naval Academy, 1983

Submitted in partial fulfillment  
of the requirements for the degree of

MASTER OF SCIENCE IN PHYSICS

from the

NAVAL POSTGRADUATE SCHOOL  
December 1992

Author:

*Stephen D. Lewia*

Stephen D. Lewia

Approved by:

*Xavier K. Maruyama*

Xavier K. Maruyama, Thesis Advisor

*Anthony A. Atchley*

Anthony A. Atchley, Co-Advisor

*Felipe Gaitan*

Felipe Gaitan, Reader

*Kai Woehler*

Kai Woehler, Chairman  
Department of Physics

**ABSTRACT**

The continuous emission of picosecond pulses of light has been observed to originate from a bubble trapped at the pressure antinode of a resonant sound field in water and in water/glycerin mixtures. The spectra of this light in several solutions has been measured with a scanning monochromator/photomultiplier detector system. The spectra are broadband and show strong emission in the UV region. A comparison of this measurement to two other independently produced spectra is made. The spectra are also modeled by a blackbody radiation distribution to determine an effective blackbody temperature and a size is deduced as if sonoluminescence were characterized by blackbody radiation.

Accession For	
NTIS CRA&I	<input checked="" type="checkbox"/>
DTIC TAB	<input type="checkbox"/>
Unannounced	<input type="checkbox"/>
Justification .....	
By .....	
Distribution /	
Availability Codes	
Dist	Avail and/or Special
A-1	

**DTIC QUALITY INSPECTED 3**

## TABLE OF CONTENTS

I.	INTRODUCTION . . . . .	1
	A. BACKGROUND . . . . .	1
	B. THESIS OBJECTIVES . . . . .	5
II.	EXPERIMENTAL ARRANGEMENT . . . . .	6
	A. BACKGROUND . . . . .	6
	B. RESONANT FLASK AND ASSOCIATED DRIVING EQUIPMENT . . . . .	6
	C. SPECTROMETER . . . . .	10
	D. DATA ACQUISITION AND DISPLAY . . . . .	15
III.	EXPERIMENTAL PROCEDURE . . . . .	19
	A. RAW DATA COLLECTION . . . . .	19
	1. Background . . . . .	19
	2. System Wavelength Resolution . . . . .	19
	3. SL in Pure Water . . . . .	21
	4. SL in 25% Glycerin Solution . . . . .	26
	5. SL in 40% Glycerin Solution . . . . .	29
	B. SYSTEM CALIBRATION . . . . .	32
	1. Background . . . . .	32
	2. Short Wavelength Calibration . . . . .	33
	3. Long Wavelength Calibration . . . . .	45
	4. System Calibration Curve . . . . .	45

5. UV Transmission in Water and 25% Glycerin Solution . . . . .	50
IV. DATA ANALYSIS . . . . .	54
A. BACKGROUND . . . . .	54
B. ANALYSIS OF RAW DATA SPECTRA . . . . .	55
C. CORRECTED SL SPECTRA . . . . .	57
1. Corrected Water Spectrum . . . . .	57
2. Corrected 25% Glycerin Spectrum . . . . .	60
3. Corrected 40% Glycerin Spectrum . . . . .	60
D. COMPARISON OF CORRECTED SPECTRA . . . . .	64
E. COMPARISON OF SL IN WATER - NPS vs UCLA . . . . .	70
F. SL SPECTRA MODELED BY A BLACKBODY RADIATION DISTRIBUTION . . . . .	70
1. SL in Water Fit to a Blackbody Distribution	73
2. SL in 25% Glycerin Fit to a Blackbody Distribution . . . . .	73
3. SL in 40% Glycerin Fit to a Blackbody Distribution . . . . .	73
4. Comparison of Blackbody Fit Data . . . . .	77
G. SL SPECTRA COMPARED TO CARLSON SPECTRA . . . . .	78
V. CONCLUSIONS . . . . .	81
LIST OF REFERENCES . . . . .	83
INITIAL DISTRIBUTION LIST . . . . .	84

## ACKNOWLEDGEMENTS

The results of this work would not have been possible without the assistance and professional expertise of many people. My advisors, Professor X.K. Maruyama and Professor A.A. Atchely, invested many dedicated hours of brainstorming and problem solving and provided invaluable guidance and direction. Their expertise with equipment operation and applied theory was essential to the success of this work. They also provided valuable exposure of the results to other members of the scientific community which created an unequalled learning experience. Joe Carlson, who was responsible for dragging me into this research, supplied me with the necessary background and motivation to get the project started. Throughout the project his correspondence and ideas were essential, as was his awesome creation, the Superflask. Dr. Felipe Gaitan devoted many hours and ideas to the project. His detailed expertise with equipment and experimental procedures provided a strict quality assurance check on all experiments and results. Felipe's help with equipment characteristics and "researching the details" made the work more complete and creditable. Professor S. Davis provided a large amount of optical expertise and advise, without which many problems would not have been solved. Jerry

Lentz also contributed significant advise and ideas for improved results, as well as experimental experience.

I am greatly indebted to Professor D. Cleary for the use of his spectrometer, calibration lamps, work area and other necessary equipment. Even though he was not directly associated with the project, his unselfishness in the lending of equipment and a work environment set an excellent example for the Physics Department. Bob Sanders also provided great assistance with equipment problems and the use of the spectrophotometer.

Several individuals at Lawrence Livermore National Laboratory provided ideas and correspondence that added to the success of the project. Darren Sweider and Philip Armatis conveyed many ideas and recommendations that resolved several problems and conflicts. Mike Moran provided professional insight and exposure of the project to the laboratory community, which was a extremely beneficial learning experience. Their assistance and ideas were greatly appreciated.

Finally, I would like to acknowledge my wife and family for their encouragement and help during my long hours at the computer. Their unselfish support made all the difference.

**DISCLAIMER**

The specific experimental equipment described in this work in no way constitutes an endorsement of these products.

## I. INTRODUCTION

### A. BACKGROUND

Sonoluminescence (SL) is a visible, soft blue light emitted from a gas bubble undergoing radial oscillations in a liquid driven by a resonant sound field. It was first observed nearly 50 years ago when photographic plates immersed in ultrasonically radiated water revealed light exposure [Ref. 1:pp.421-424]. SL was also observed in water and other liquids exposed to intense sound fields that induced cavitation in the liquids [Ref. 2:pp.290-292]. This "transient" cavitation produced random pulses or clouds of light that seemed to be emitted during chaotic oscillations and collapse of the cavitating bubbles [Ref. 3:p.388]. Many theories were proposed to explain SL. However, experimentally validating any of these theories proved to be difficult, if not impossible, because of the transient nature of the phenomenon. Physical bubble features, such as radius, temperature, and internal pressure, or the spectrum of the emitted light, could not be accurately determined. Without these physical bubble features, the mechanism behind SL could not be determined.

In 1990, Gaitan discovered a method to isolate a single, stable, cavitating bubble that emitted light in what visually

appeared to be a continuous output [Ref. 4:p.3166]. A small air bubble, approximately 20 microns in radius, was levitated in water or water/glycerin mixtures at the pressure antinode of a resonant sound field. The sound field in the liquid was produced by driving a glass flask with piezoelectric transducers at a resonant frequency. The resonating flask produced a standing wave in the liquid, which caused the suspended air bubble to oscillate radially. When driven with sufficient amplitude, the bubble emitted SL. The light emission could be made to continue indefinitely. SL emission has been sustained for several hours at the Naval Post Graduate School and at Lawrence Livermore National Laboratory (LLNL).

It was soon discovered, by viewing the light emission with a photomultiplier tube, that the emission was actually pulses of light of very short duration occurring once every acoustic period. Radius versus time curves of the bubble motion were obtained from a laser scattering technique and showed the bubble cycle and the timing of SL emission relative to the sound field. Figure 1 shows the results of these measurements [Ref. 4:p.3180]. The bubble oscillates radially with the acoustic cycle and SL is emitted each time the bubble undergoes a rapid collapse in response to an increasing sound field driving pressure.

The isolation of a single, stable bubble emitting SL continually was an important discovery and enabled a more

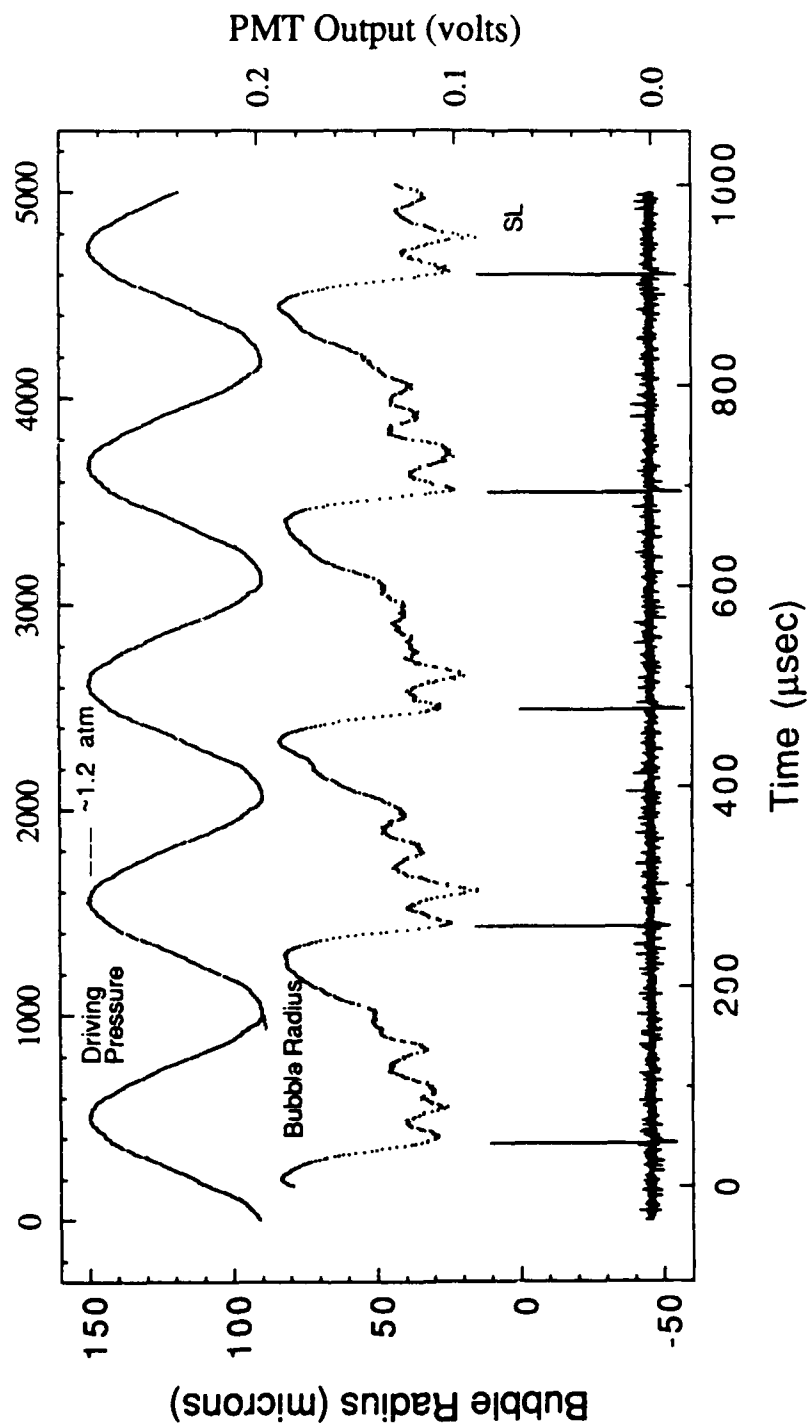


Figure 1 SL Physical Characteristics

detailed study of the phenomenon. Putterman showed that the SL flash duration was less than 50 ps by comparing it to a pulsed laser flash [Ref. 5:p.3061]. He also produced an optical spectrum for SL in pure water which indicated a large part of the light produced by SL was in the ultraviolet (UV) region [Ref. 6:p.1192]. His spectrum was continuous, with no evidence of spectral lines at a resolution of 1 nm. The SL spectrum was still increasing in intensity at the UV limit of his system. Because the light emitted was largely in the UV region at photon energies above 6 eV (200 nm), Putterman concluded that a focusing of the ambient sound field energy of over 11 orders of magnitude was involved in producing SL [Ref. 6:p.1183]. A reliable optical spectrum would reveal important clues about the mechanism producing SL.

The physical limits of SL make an accurate spectral measurement difficult. SL is produced from an extremely small source, suspended in a liquid medium. The liquid acts as a filter which establishes a lower wavelength limit to the spectral measurement. The intensity of a single SL flash is high. However, because the pulse length is very short compared to the repetition frequency, the absolute average intensity of SL measured is low compared to the total background noise. The low average intensity dictates the use of signal processing and enhancement techniques to extract the signal from background noise. The SL bubble is often unstable over the time period of a spectral measurement. The bubble

frequently changes position and intensity, which may greatly affect the outcome of a measurement. Getting a sufficient amount of light from the SL source to the input of a measurement device is also a difficulty that must be overcome to produce an accurate optical spectrum. Because of these difficulties, each of which may account for significant uncertainties, it is important that several independent measurements of the SL spectrum be made before a final result is agreed upon.

#### **B. THESIS OBJECTIVES**

The goal of this work is to report the results of an experiment conducted to determine the optical spectrum of SL in water. These results will be compared to previous work by Putterman, et al. [Ref. 6], and to the results obtained in another independent measurement with a slightly different technique, et al. [Ref. 7]. It is hoped that this measurement comparison will produce a spectrum that will aid in describing the mechanism producing SL.

This thesis will also compare the SL spectrum in water to that of two water/glycerin mixtures. A significant difference between the spectra has been observed. The resulting water and water/glycerin spectra closely resemble blackbody radiation distributions of different temperatures and sizes. The spectra will be modeled by a blackbody distribution to identify any possible correlation.

## **II. EXPERIMENTAL ARRANGEMENT**

### **A. BACKGROUND**

Recording the spectra of SL requires equipment and techniques that minimized the amount of light attenuated from the SL source, especially in the UV region, and allows a sufficient signal to reach a detector. The equipment used to produce SL spectra for this thesis are grouped into three general categories:

1. Resonant flask and associated driving equipment
2. Spectrometer
3. Data acquisition and display

Each of these equipment groups will be discussed separately since each provides an important function that uniquely affects the resulting spectra.

### **B. RESONANT FLASK AND ASSOCIATED DRIVING EQUIPMENT**

The resonant flask is the apparatus in which sonoluminescence was produced. A 500 ml, spherical, Pyrex flask with a two inch diameter neck was used in this experiment. Eight cylindrical piezoelectric transducers were cemented in symmetrically opposed pairs around the perimeter of the flask. Even though one transducer could, in practice, produce a sufficient signal for SL, the eight transducer

arrangement was chosen to produce a strong, stable, symmetric pressure wave inside the liquid filled flask. The multiple transducer arrangement was hoped to minimize asymmetries. The transducers were driven by a sinusoidal wave from a function generator (HP 8904A) through an audio amplifier (Techron 5530). Figure 2 shows the resonant flask and associated driving equipment.

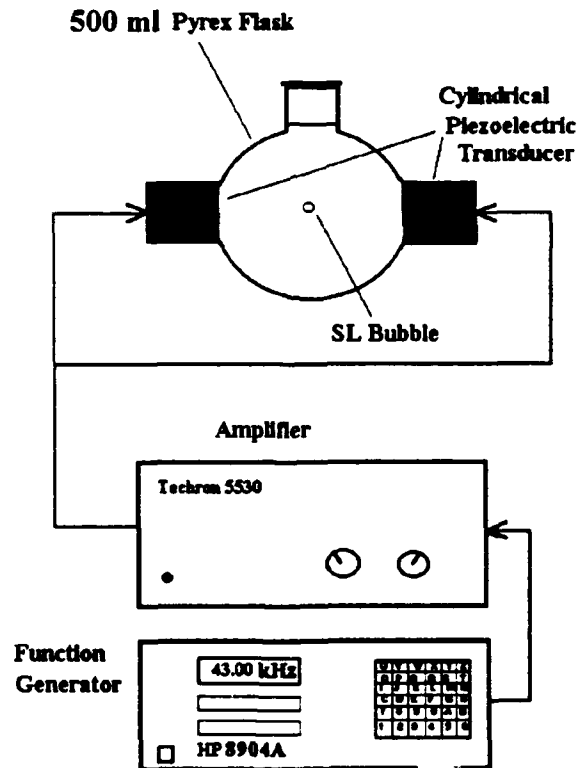


**Figure 2** Equipment Used to Produce SL

The flask was filled with degassed water or a degassed water/glycerin mixture. By selecting the appropriate driving frequency and amplitude, the flask was made to resonate with sufficient force as to produce high amplitude spherically symmetric standing waves in the liquid. An air bubble injected with a hyperdermic needle into the flask will immediately migrate to the pressure antinode of the standing wave, approximately in the center of the flask. The bubble oscillates radially in response to the resonant driving force. When the driving force is increased the bubble will shed or attract smaller bubbles, assuming a size optimal for the environment. When driven with sufficient amplitude the bubble will produce SL pulses continually. All the conditions necessary to cause SL are not yet fully understood.

A miniature hydrophone was initially used to quickly locate the resonant frequencies of the liquid/flask combination. The hydrophone, approximately 1/8 of an inch in diameter, was positioned into the liquid and the output signal was observed with an oscilloscope. Maximum hydrophone response indicated the resonant frequencies. The resonant driving frequencies depend upon the type of liquid in the flask, flask material and size, and the temperature of the liquid.

Once SL was produced, the overall intensity could be varied by changing the frequency and amplitude of the driving signal. Putterman claimed that the SL spectrum was consistent

over a large variation in bubble intensity [Ref. 6:p.1183]. This thesis will support that claim. However, bubble stability (i.e., bubble lateral movement and intensity fluctuations) are a direct function of the driving signal amplitude. A bright bubble (i.e., driven hard) is usually not stable enough over a measurement period (10 to 15 minutes) to produce acceptable spectra.

Bubble stability during a measurement period is very important since a scanning method was used to analyze the spectrum, as will be discussed later. A bubble driven too hard jumps around or even disintegrates, and ruins the measurement. However, an intensely bright SL bubble is advantageous because more light gets to the detection equipment which requires as much light as possible. A compromise between brightness and stability must be reached by varying the frequency and amplitude of the driving signal in order to produce adequate results. An acceptable combination was determined mostly by trial and error.

Liquid purity also affected bubble stability. Particulate matter suspended in the liquid interferes with the sound field and the oscillating bubble, and can cause bubble movement and short term intensity shifts. Therefore, the liquid medium must be as clean as possible. Particulate matter was minimized by filtering the liquid and cleaning the flask regularly. With practice, a stable, adequately intense SL

bubble was produced that provided sufficient light for a spectral measurement.

SL can only be produced in liquids that have been properly degassed. Solutions were degassed in the resonant flask by attaching a vacuum pump to a stopper inserted into the neck of the flask. Pure water was degassed until no rising bubbles were visible in the flask and the flask began to get cold. Pure water must be degassed considerably before SL is possible. In general, water/glycerin mixtures require less degassing. However the amount of degassing for successful SL in glycerin mixtures can vary and the reason is uncertain. SL can be achieved in mixtures that are degassed very little, i.e., just until the initial surge of bubbles subsides, or degassed a lot as with water. It seemed difficult to produce SL in mixtures that were degassed to an intermediate state. Glycerin mixtures were degassed in the same manner as water for this experiment.

### C. SPECTROMETER

The spectrometer used in this experiment was a 0.3 m, scanning monochromator with a rotating grating (Acton Research Corp. model VM-503). The grating rotation was controlled by a computer through a power supply (ARC Model 747) to a stepper motor and could be adjusted to step through a set wavelength interval and view a particular wavelength for a selected time interval. The grating used was an AlMgF<sub>2</sub> coated, plane

grating of 1200 grooves/mm blazed for a wavelength of 300 nm. The output of the spectrometer was collected with a photomultiplier tube (PMT). The PMT was a 30 mm, end window type (Thorn EMI 9798QB) with an S-20 response and a quartz window for greater UV sensitivity. The PMT output was preamplified and fed into a lock-in amplifier (Stanford Research Systems model SR 530), whose operation will be discussed later.

SL light was collected at the source with a 600  $\mu\text{m}$  diameter core silica clad, silica, single mode fiber optic cable (3M FG-600-UAT). The fiber, about 1 m long, was cleaved flat at both ends. One end was positioned inside the flask and maneuvered with an XYZ stage to within 0.5 cm of the SL bubble. The other fiber end was positioned into the entrance slit of the spectrometer, at the slit plane. The fiber was centered in the slit plane and locked into position with a special adapter. The adapter also prevented outside light from entering the slit above and below the fiber. Figure 3 shows the arrangement of the spectrometer and resonant flask equipment.

An optical fiber was chosen over a lens system to transfer the light from the SL bubble to the spectrometer. The fiber provided the following advantages:

- The index of refraction of the fiber (1.5) closely matched that of the liquid medium (1.3 for water). A more efficient coupling of the light to the spectrometer was

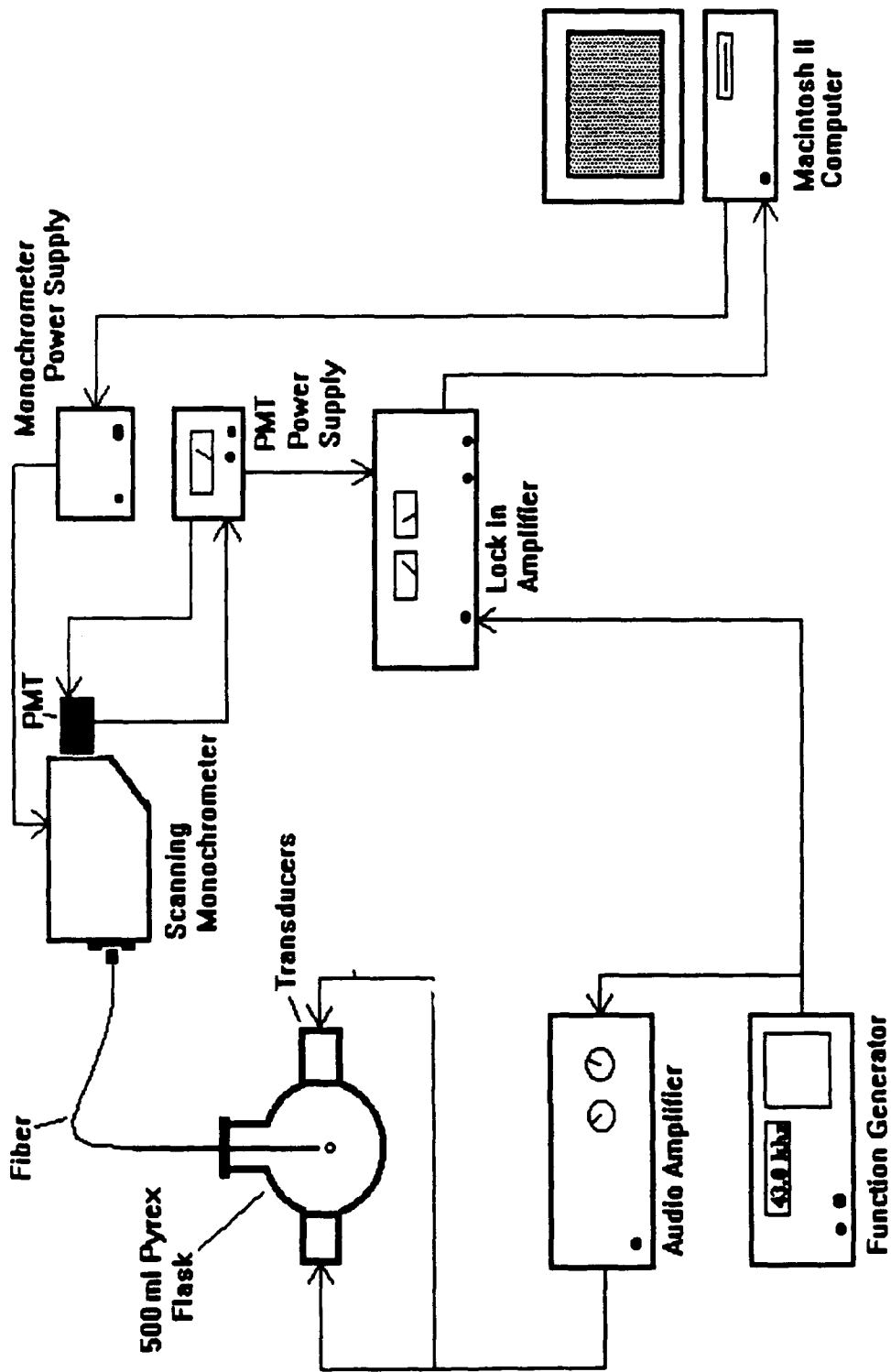


Figure 3 Experimental Equipment Setup

achieved through the fiber in the liquid than through the air to the slit.

- Because of its finite acceptance angle, the fiber allowed for small changes in bubble position without adversely affecting the recorded bubble spectra. Changes in bubble position, if transmitted to the spectrometer entrance plane cause an invalid shift in the wavelength of the recorded light. The fiber, being much larger than the SL bubble, allowed significant bubble movement while transferring stable light to the spectrometer entrance plane. A lens system would translate bubble movement to the spectrometer plane as the bubble moved in and out of the focal point of the lens.
- The fiber was easily maneuvered in the resonant flask to within about 0.5 cm of the bubble, to collect as much light as possible. The fiber size and ability to get close to the bubble resulted in a greater solid angle of light observed as compared to what could be imaged through the flask neck to a lens system. Because the fiber could be positioned close to the bubble, less light was attenuated by the liquid, resulting in a stronger signal for the spectrometer.

A silica clad, silica core fiber was chosen over other fiber types to extend the SL spectrum as far as possible into the UV region. The use of a fiber, however, introduced the following disadvantages to a spectral measurement:

- The fiber attenuated more light at the UV limit of the system as compared to air.
- Because the fiber acts as the entrance aperture to the spectrometer, the relatively large fiber diameter equates to a poor spectral resolution.

Figure 4 compares a D<sub>2</sub> lamp spectrum recorded through the 600 μm fiber and through a 600 μm slit with no fiber. Significant signal is lost by the fiber. However, the advantages of light collection with a fiber, for a reliable spectral measurement,

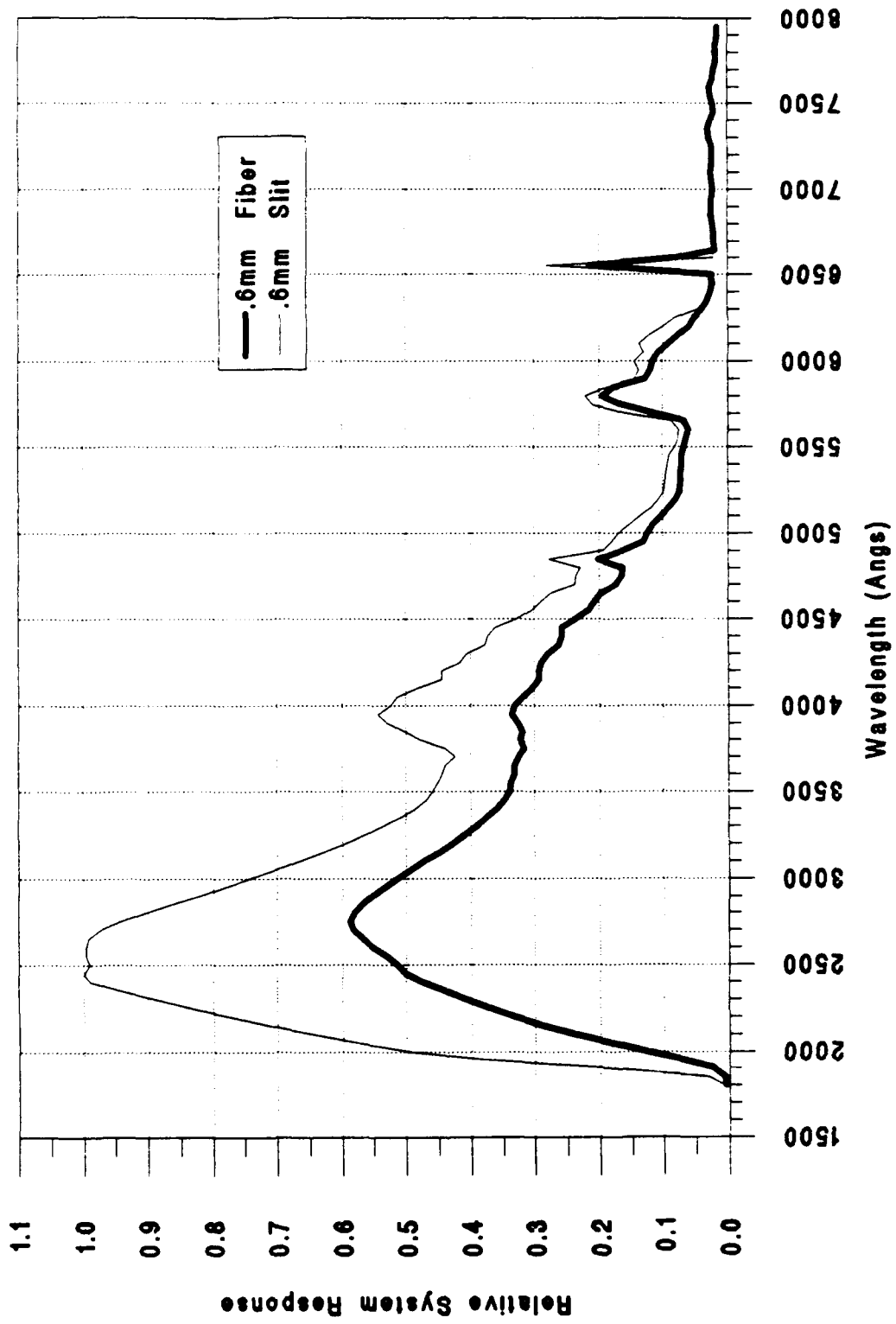


Figure 4 Fiber vs Slit Response to a D2 Lamp Source

make up for the signal loss. The system spectral resolution and its importance for a meaningful measurement will be evaluated later.

#### **D. DATA ACQUISITION AND DISPLAY**

The output of the PMT was preamplified and sent to the input of a lock-in amplifier. The function generator output was fed to the lock-in amplifier as a reference signal (Figure 3). Since SL flashes are produced once each acoustic period, the reference signal identifies the SL flash frequency. The lock-in amplifier analyzes the PMT signal and identifies a frequency component produced by the periodic SL flashes that matches the reference signal. The amplitude of this frequency component is proportional to the number of SL photons received by the PMT. Thus, the DC output of the lock-in amplifier is directly proportional to the number of SL photons measured by the PMT. This method improved the signal to noise ratio of the system by a factor of 350 as compared to the PMT output signal alone. The SL signal from the lock-in output is roughly 35 times the noise background. Figure 5 shows a typical SL spectrum plotted against an average background signal. The SL signal dominates the lock-in amplifier output signal.

The output signal from the lock-in amplifier was sent to an analog to digital converter board installed in a Macintosh computer (Figure 3). The computer sampled the DC signal

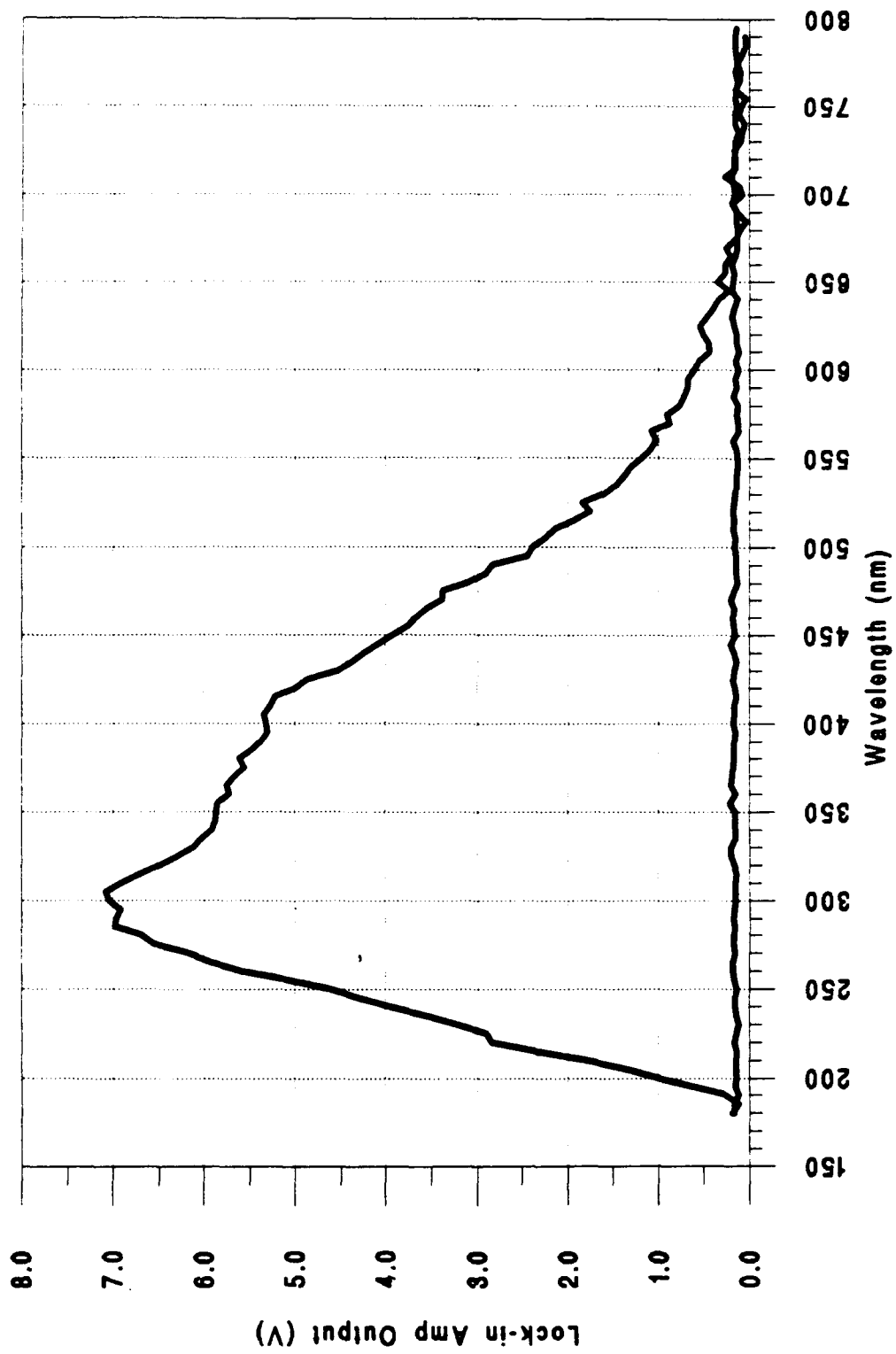


Figure 5 Typical Bubble Spectrum vs Background Noise

20,000 times for a specified sample time interval (20  $\mu$ s) at a specific wavelength, and recorded an average value based on these samples. The number of samples and the sample time interval were controlled by user inputs to the computer.

The same computer also controlled the spectrometer scan rate and wavelength interval. User inputs determined the beginning and ending wavelength scan values, and the wavelength interval between successive measurements. Thus, SL spectrum values were sampled and averaged at individual wavelengths and the average value was recorded prior to scanning to the next wavelength. The recorded value was proportional to the number of photons received by the PMT at a particular wavelength. The recorded values were collectively displayed on the computer monitor as a graph of output voltage (photon count) vs wavelength. The recorded values were also saved in data files for later data analysis.

Producing a stable bubble for long time periods (10 - 15 min) was crucial to obtaining an acceptable SL spectrum with the equipment described above. Any change in bubble intensity during the recording period will result in erroneous output data for the wavelengths being recorded. The relative photon count between successive wavelength values must be recorded from SL light at a constant intensity. Fortunately, small, random intensity fluctuations that occur during the averaging period will be averaged out by the computer sampling technique. However, large intensity shifts that occur for

significant time periods will cause false notches or peaks in the recorded spectra. Therefore, the output of the lock-in amplifier is monitored visually with a multimeter. Large intensity shifts can be visually detected and the run can be discarded. Recorded spectra are later averaged together to ensure spectrum structure is not lost, since some intensity shifts may still affect the data. The methods and experimental setup described above attempted to minimize the effects of intensity variation errors. Intensity errors will be evaluated statistically later.

### III. EXPERIMENTAL PROCEDURE

#### A. RAW DATA COLLECTION

##### 1. Background

The equipment setup was designed to maximize the amount of SL light collected over as extensive a wavelength range as possible with the equipment available. Precautions were also taken to ensure that spectrum errors due to intensity fluctuations were minimized. Raw data was collected for SL in degassed water and two degassed glycerin/water solutions. All solution mixtures stated are by volume. Each of these measurements will be discussed separately. First, the system wavelength resolution was determined in order to properly select the wavelength scan interval of the spectrometer.

##### 2. System Wavelength Resolution

The system wavelength resolution was determined by viewing the spectrum produced by a green Helium - Neon laser (543.5 nm) at 10 Å increments. The observed line width at full width/half maximum was about 7 nm, as indicated in Figure 6. Therefore the system resolution is about 7 nm. Previous work on SL has shown no spectral line structure at a resolution of 1 nm [Ref. 6:p.1184]. Since we are not concerned with spectral line structure, a wavelength scan

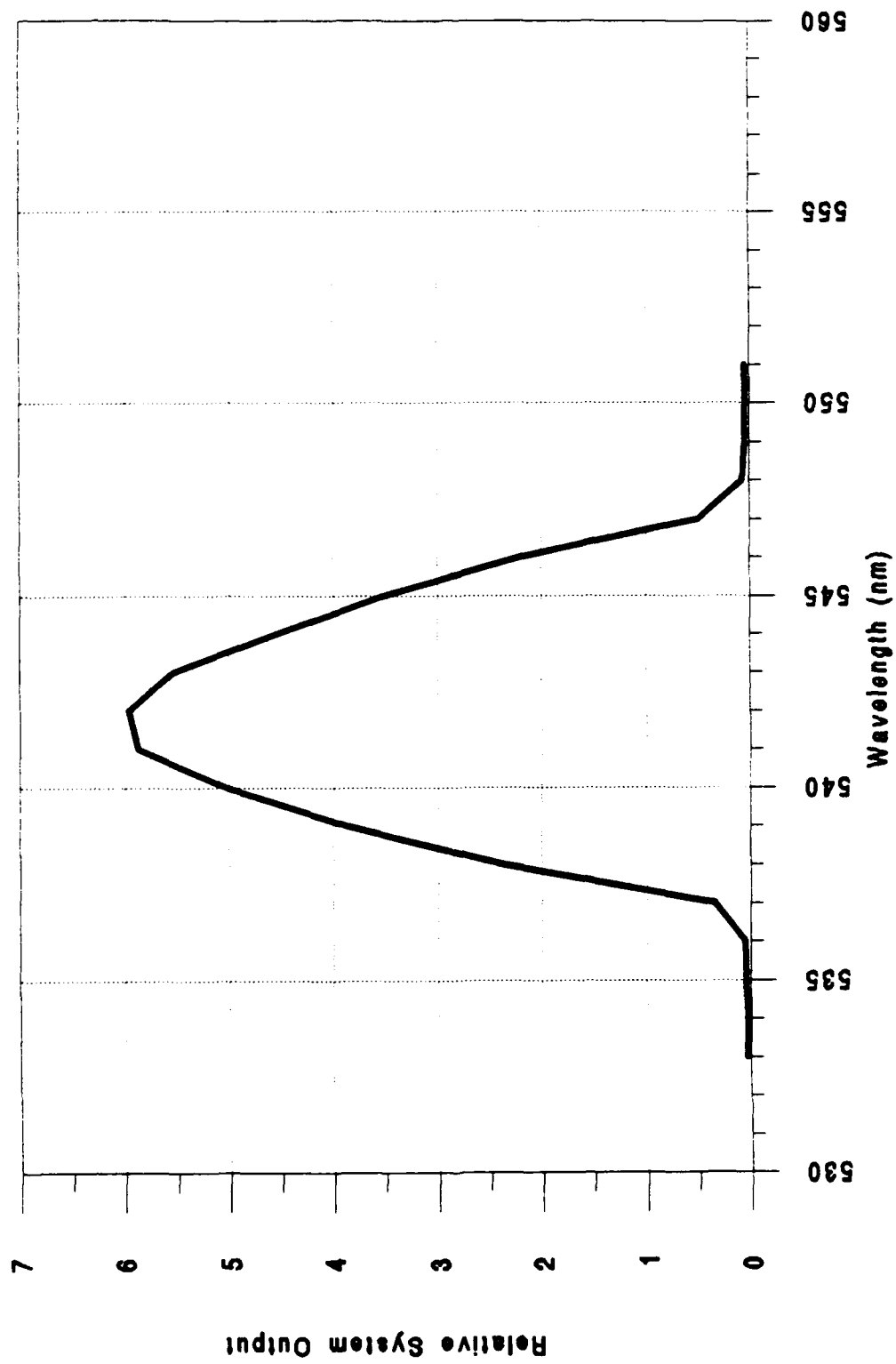


Figure 6 System Response to a Green HeNe Laser

interval of 5 nm was chosen for raw data collection so that successive measurements would overlap within the system resolution. A smaller scan interval could have been selected, however doing so would have greatly increased the time required to complete an entire wavelength scan of SL, with little gain in spectral information. Difficulty in maintaining bubble stability for long time periods dictated using the shortest total scan time possible. Therefore a 5 nm wavelength scan interval was deemed sufficient.

### **3. SL in Pure Water**

Water was degassed in the resonant flask. SL was achieved at a frequency of about 43 kHz and a driving signal amplitude of 13 VAC(RMS). The PMT high voltage was set to 1000 V. The spectrometer was adjusted to scan at 5 nm wavelength intervals, from 180 nm to 800 nm. The computer was set to collect 20,000 samples of the lock-in output signal at 20  $\mu$ s intervals (i.e., 400 ms total) for each wavelength. The computer recorded the average of these 20,000 samples as a voltage level (photon count) for each wavelength. The fiber was positioned 0.5 cm from the bubble. The lock-in amplifier was set with a 3 s time constant and a 10 mV sensitivity. The time between successive wavelength readings was a few seconds, allowing the lock-in to stabilize on the next wavelength before data was recorded. Figure 7 shows a typical raw data spectrum for SL in water. This spectrum is uncorrected for system

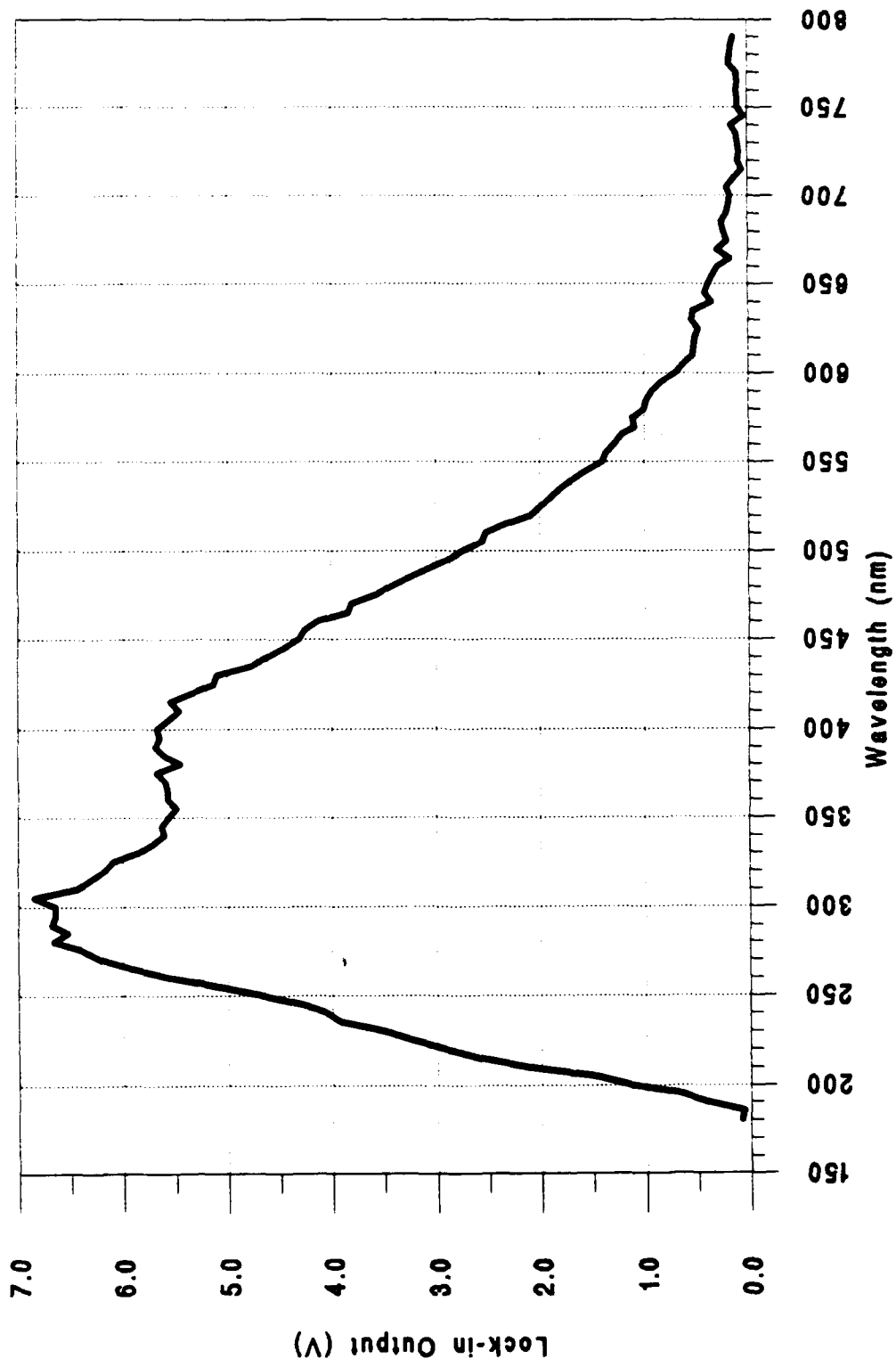


Figure 7 Typical SL Raw Data Spectrum in Water

component response deviations at various wavelengths, which will be accounted for later. Seven acceptable spectra were recorded for water. The spectra were averaged and a standard deviation was calculated. Figure 8 shows the mean raw data SL spectrum for water with error bars indicating the standard deviation in the seven data sets. The size of the error bars is an indication of how much the intensity of SL can vary between different scans.

At the completion of each scan, the driving frequency and amplitude were readjusted to ensure a stable bubble for the next scan. The readjustment was almost always necessary. The changes in frequency were on the order of one percent and voltage amplitude changes were on the order of ten percent. These changes resulted in a factor of two range in peak intensity between the seven runs.

The seven individual scans were then each normalized to one at their peak amplitudes. The mean and standard deviation of the normalized spectra were calculated. Figure 9 shows the mean of the normalized spectra with the standard deviation as error bars. This plot represents the variation in the spectrum shape between the seven scans. The shape is very consistent, even though there were significant differences in the run to run intensity among the seven scans. The individual spectra exhibit nearly the same spectral shape with the peak intensities being observed at the same wavelength.

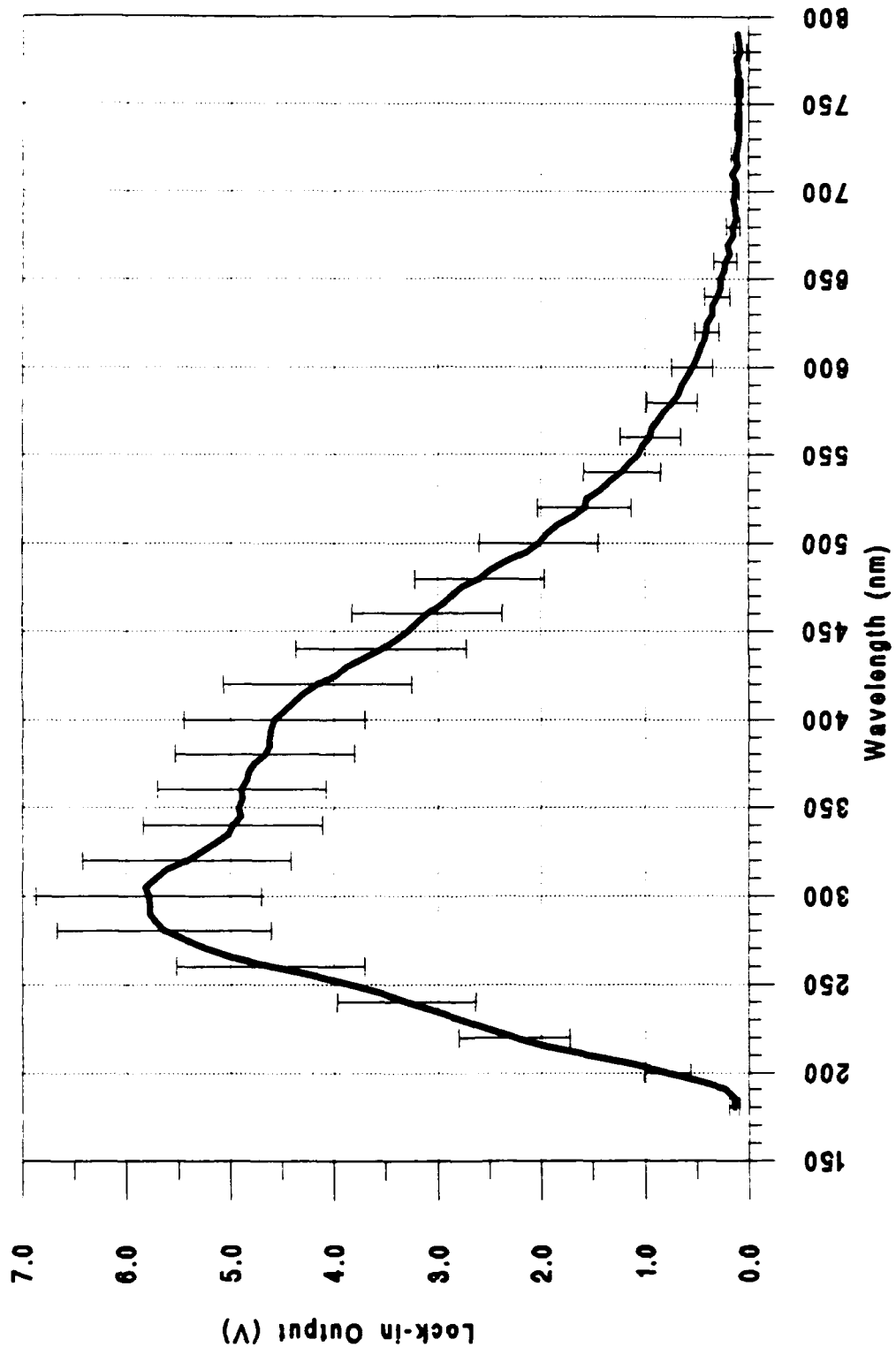


Figure 8 Average Water Spectrum - Raw Data

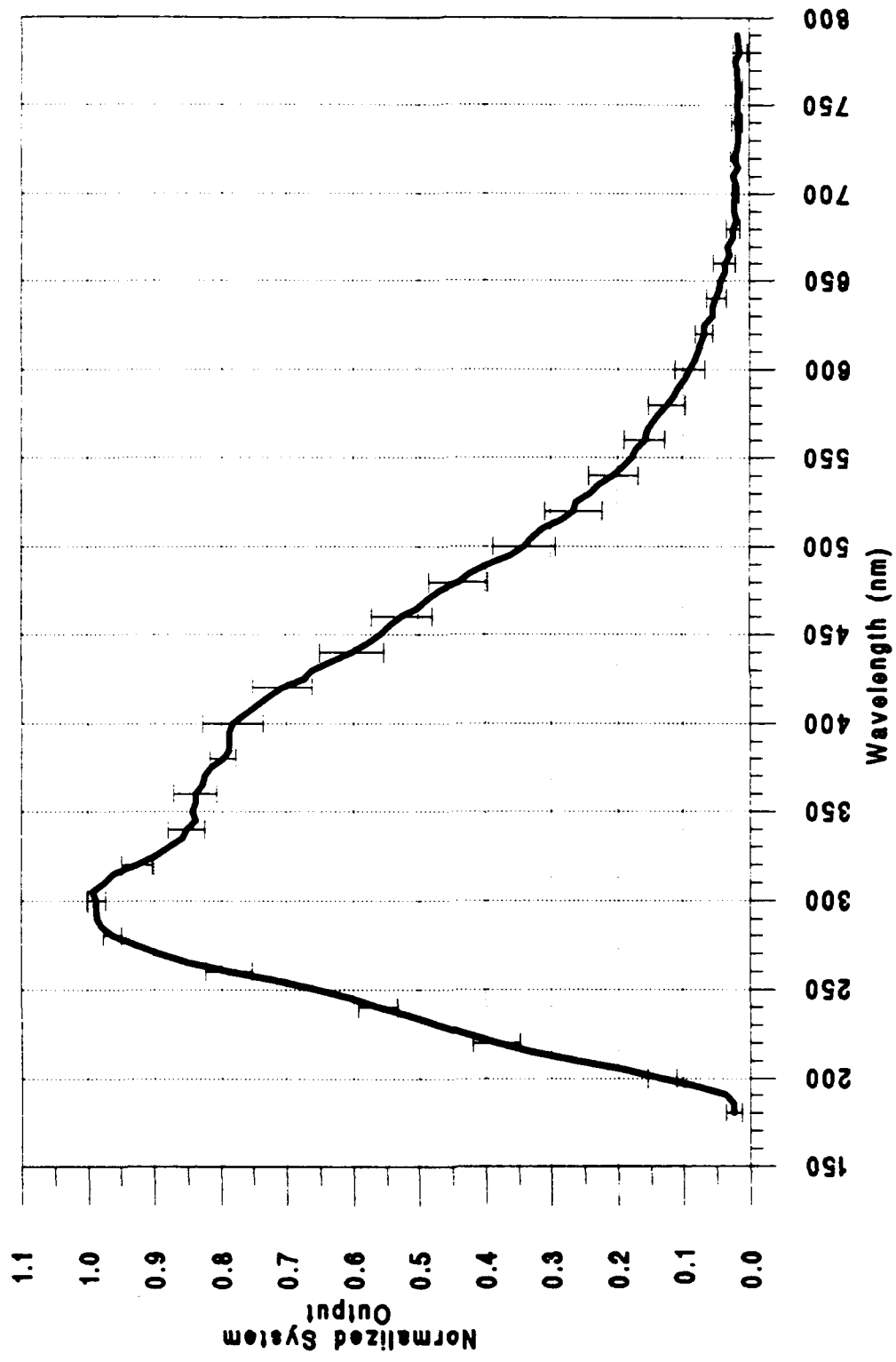


Figure 9 Normalized Water Spectrum - Raw Data

#### 4. SL in 25% Glycerin Solution

A solution of 25% glycerin and 75% water was degassed in the resonant flask. Compared to pure water, SL was achieved at a slightly higher driving frequency of about 46 kHz and the same amplitude of 13 VAC. Scan interval, wavelength range, PMT voltage, number of samples, sample time, fiber distance, and lock-in settings were set identical to those used in the water spectra. Eight acceptable spectra were produced, and again it was necessary to adjust the driving frequency and amplitude between individual scans. The driving signal changes were of the same magnitude as in pure water. The eight scans were averaged and the standard deviation was calculated. Figure 10 shows the mean of the seven scans plotted with the standard deviation as error bars. Again, a large variation in intensity between different scans was observed, as indicated by the size of the error bars. The intensity variations were again due to adjustments in the frequency and amplitude of the driving signal that were required between successive scans.

The individual spectra were also normalized to one at their peak values. The normalized spectra were averaged and a standard deviation was calculated. Figure 11 shows the mean of the normalized spectra for SL in a 25% glycerin solution with the standard deviation plotted as error bars. The spectrum shape is again very consistent between scans, even with large run to run variations in SL intensity.

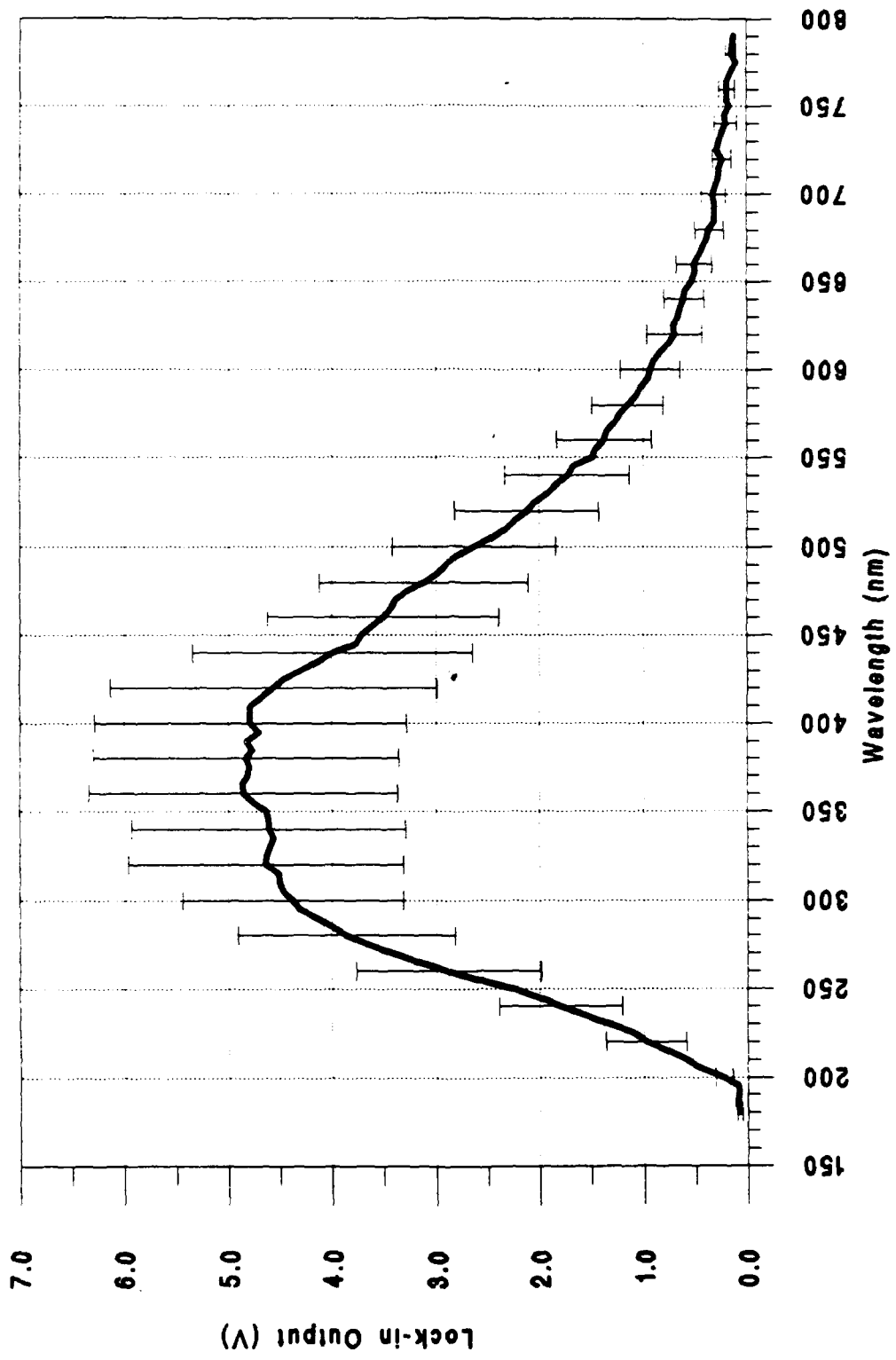


Figure 10 Average 25% Glycerin Solution Spectrum - Raw Data

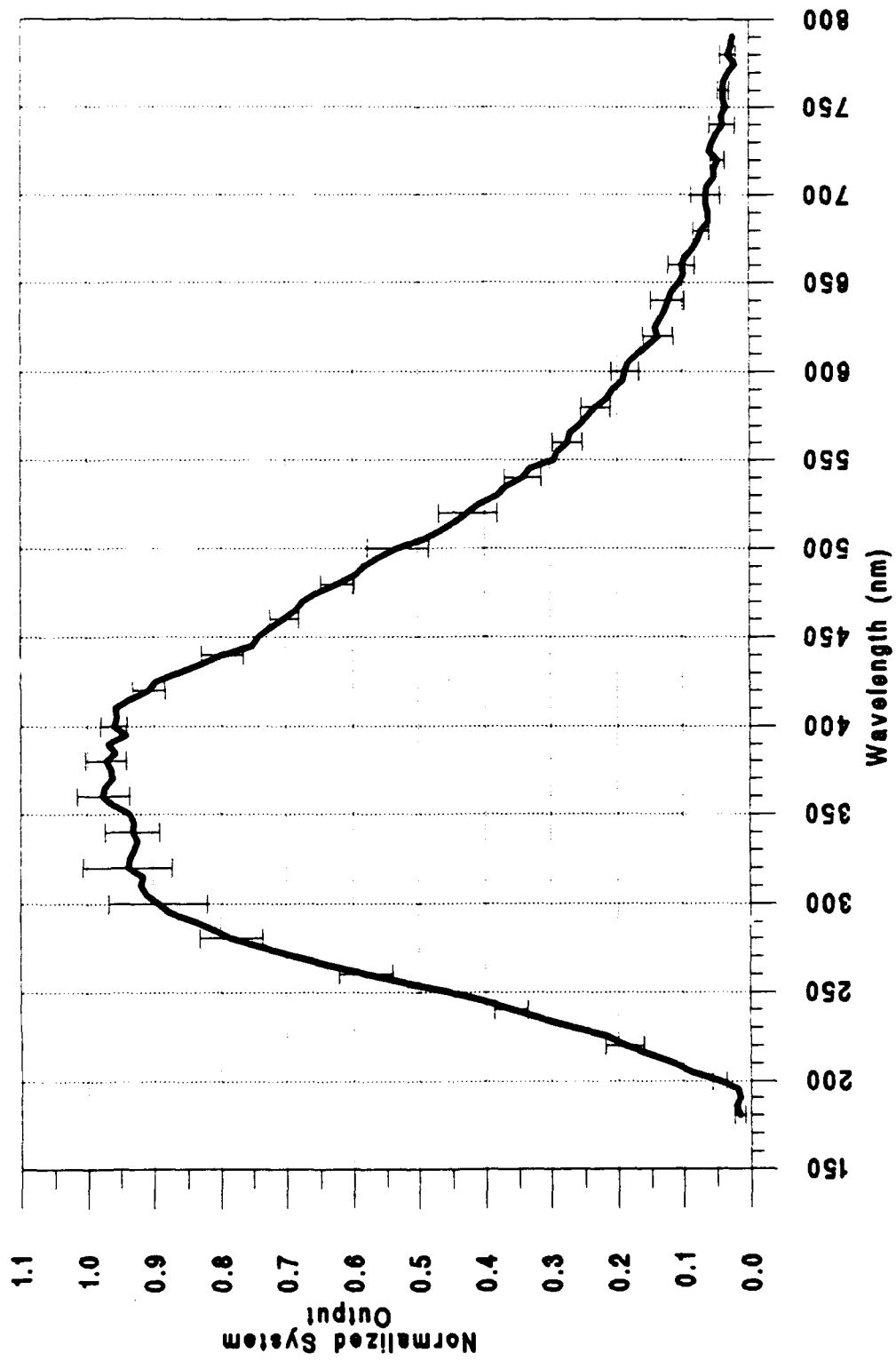


Figure 11 Normalized 25% Glycerin Spectrum - Raw Data

## 5. SL in 40% Glycerin Solution

A solution of 40% glycerin and 60% water was degassed in the resonant flask. SL was achieved at a driving signal frequency of about 52.5 kHz and amplitude of 13 VAC. It was not possible to produce an intensely bright bubble, and the bubble was highly unstable. The system configuration was identical to that stated above in the water SL section except the fiber was 0.3 cm from the bubble.

Because of bubble stability problems, only five acceptable scans were produced. The mean of these five scans is shown in Figure 12 along with the standard deviation. There is a fairly large variation in intensity from run to run, especially at the longer wavelengths. The intensity shift was again due to adjustments in driving signal frequency and amplitude of roughly the same order of magnitude as that for water. The upper wavelength limit for each scan was cut back from 800 nm to 600 nm to speed up the scan rate, since the bubble was very unstable.

Each run was then normalized. The mean of these normalized scans is plotted in Figure 13. Again the error bars indicate the standard deviation of the normalized runs or the variation in the shape of the curve. The variation in the shape of the curve is larger than the water and 25% glycerin data although all the curves peak at nearly the same wavelength.

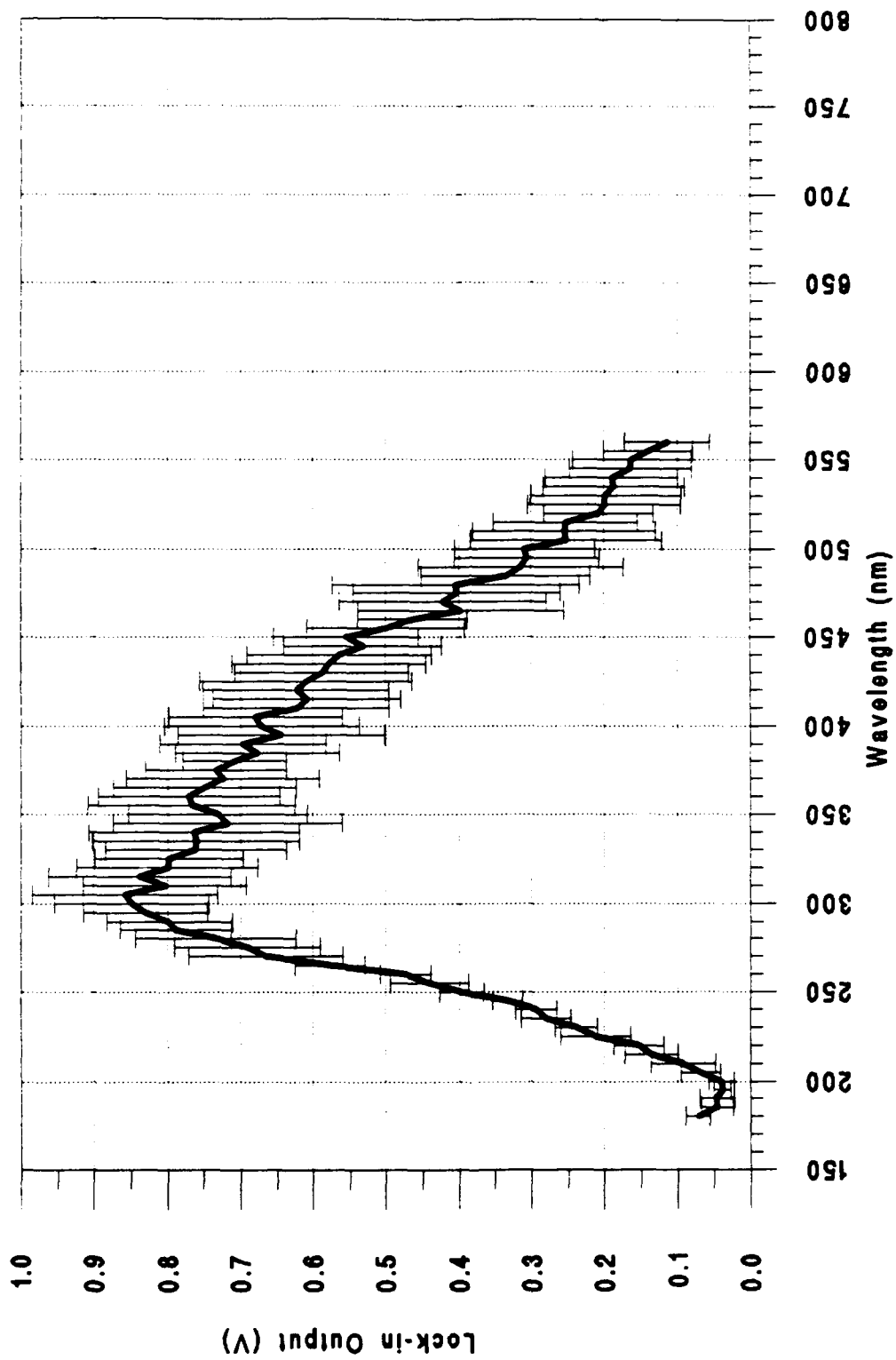


Figure 12 Average 40% Glycerin Spectrum - Raw Data

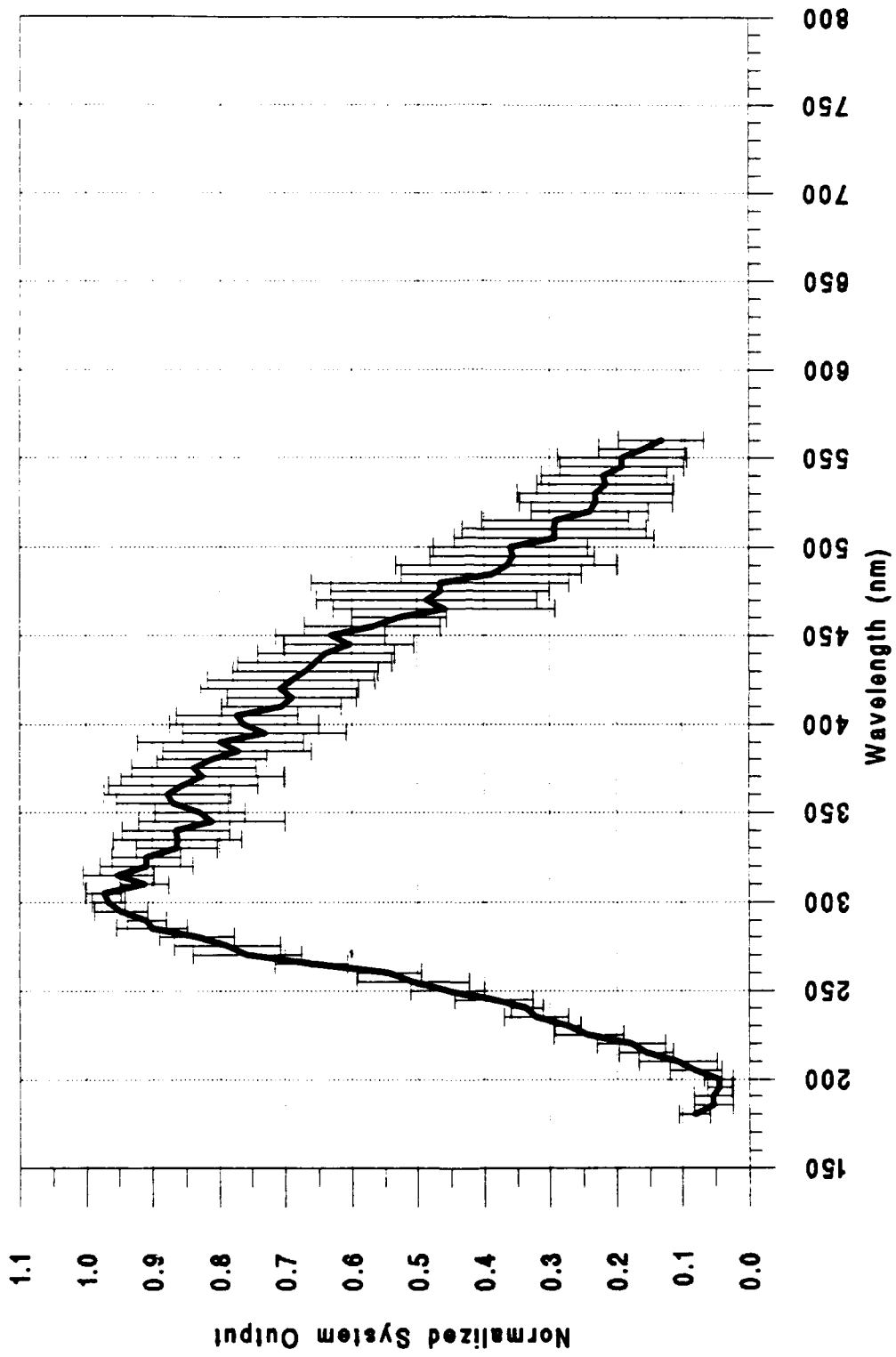


Figure 13 Normalized 40% Glycerin Spectrum - Raw Data

Table 1 summarizes the driving signal characteristics for SL in the various solutions.

TABLE (1)

Solution	Frequency (kHz)	Amplitude (VAC)
Water	43.0	13
25% gly/75% water	46.0	13
40% gly/60% water	52.5	13

## B. SYSTEM CALIBRATION

### 1. Background

The spectral response of various system components (i.e., PMT, grating, fiber) is not the same. Determining the total system spectral response characteristics and correcting for them was necessary to determine the SL spectrum. The raw data curves presented above must be corrected for variations in the system spectral response to determine the true SL spectrum.

This experiment was set up to determine not only the shape of the SL spectrum, but also the total SL output power. The system spectral response was determined by comparing the system response of two known light sources to that of their known spectra. In the shorter wavelengths (200 nm - 400 nm) a Deuterium (D<sub>2</sub>) lamp was used as a calibration source to

determine the system spectral response and corrections. The D<sub>2</sub> lamp was also used to calibrate the system spectral amplitude (Y axis) for absolute output power. A Tungsten-Halogen (TH) lamp was used as a calibration source to determine the system spectral response at the longer wavelengths (400 nm - 750 nm). The two calibrations were overlapped to produce a final system correction curve. The final system correction curve was used to correct for the nonuniform response of the various system components. The long and short wavelength calibrations will be discussed separately. The calibration of the SL spectra will also consider UV light absorption effects in water and in a 25% glycerin/75% water solution.

## **2. Short Wavelength Calibration**

Calibration to obtain the system spectral response and the Y axis absolute output power for the wavelength region 200 nm to 400 nm was accomplished by use of a D<sub>2</sub> lamp (EG&G Gamma Scientific). Spectral irradiance values, in  $\mu\text{Watts}/\text{cm}^2*\text{nm}$ , supplied with the lamp provided a known source and power output with which to determine the system response to light input and correct for all system component responses. Figure 14 shows the D<sub>2</sub> lamp calibration data. The spectral irradiance data is valid at a distance of 50 cm from the lamp.

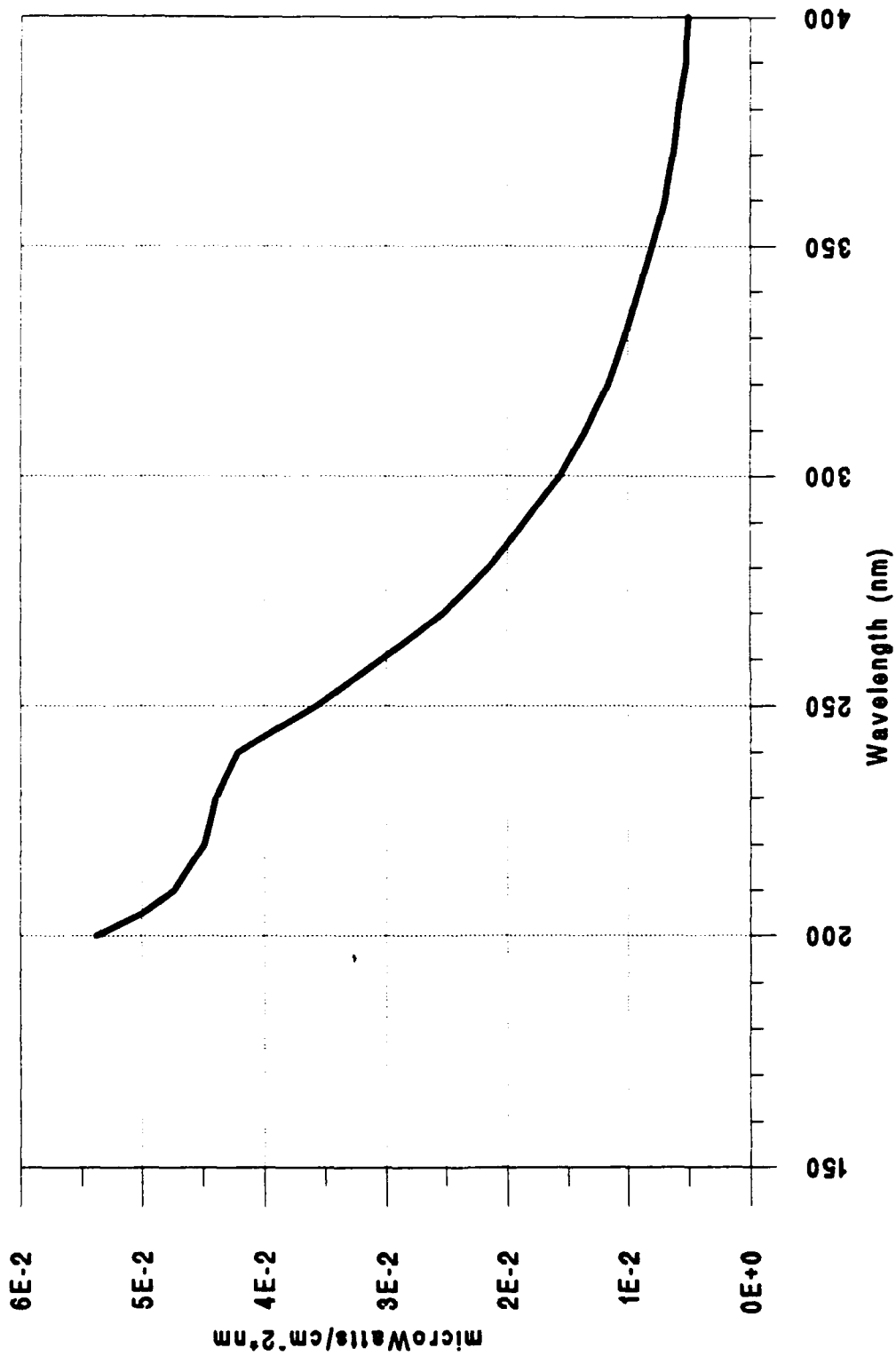


Figure 14 D2 Lamp Calibration Data

The D<sub>2</sub> lamp was placed 50 cm from the fiber entrance. Alignment of the fiber to the lamp was determined by locating the fiber XY position that generated a maximum system output amplitude at 300 nm. In order to generate correction factors for the raw SL data, the system was configured identically to that presented in the raw data section; i.e., same PMT supply voltage, same sample time and number, same wavelength interval, and identical lock-in amplifier settings.

In order to calibrate the system and the lock-in amplifier output amplitude (Y axis), a light chopper was positioned between the D<sub>2</sub> lamp and the fiber. The light chopper frequency was set at 2000 Hz. The light chopper output frequency, which was the actual flash frequency obtained from a photodetector within the light chopper, was used as a reference signal input to the lock-in amplifier.

However, the average output power of the D<sub>2</sub> lamp was lowered by the light chopper. The duty cycle of the light chopper is one half, i.e., the slits in the wheel of the light chopper are identical to the spaces between them. A correction for this effect was determined by comparing the response of the system with and without the light chopper, not using the lock-in amplifier or filters. Figure 15 shows the D<sub>2</sub> lamp spectrum with and without the light chopper. Figure 16 shows the correction curve for the light chopper, as derived by division of the two curves in Figure 15. The curve is flat, as it should be, with no wavelength dependence.

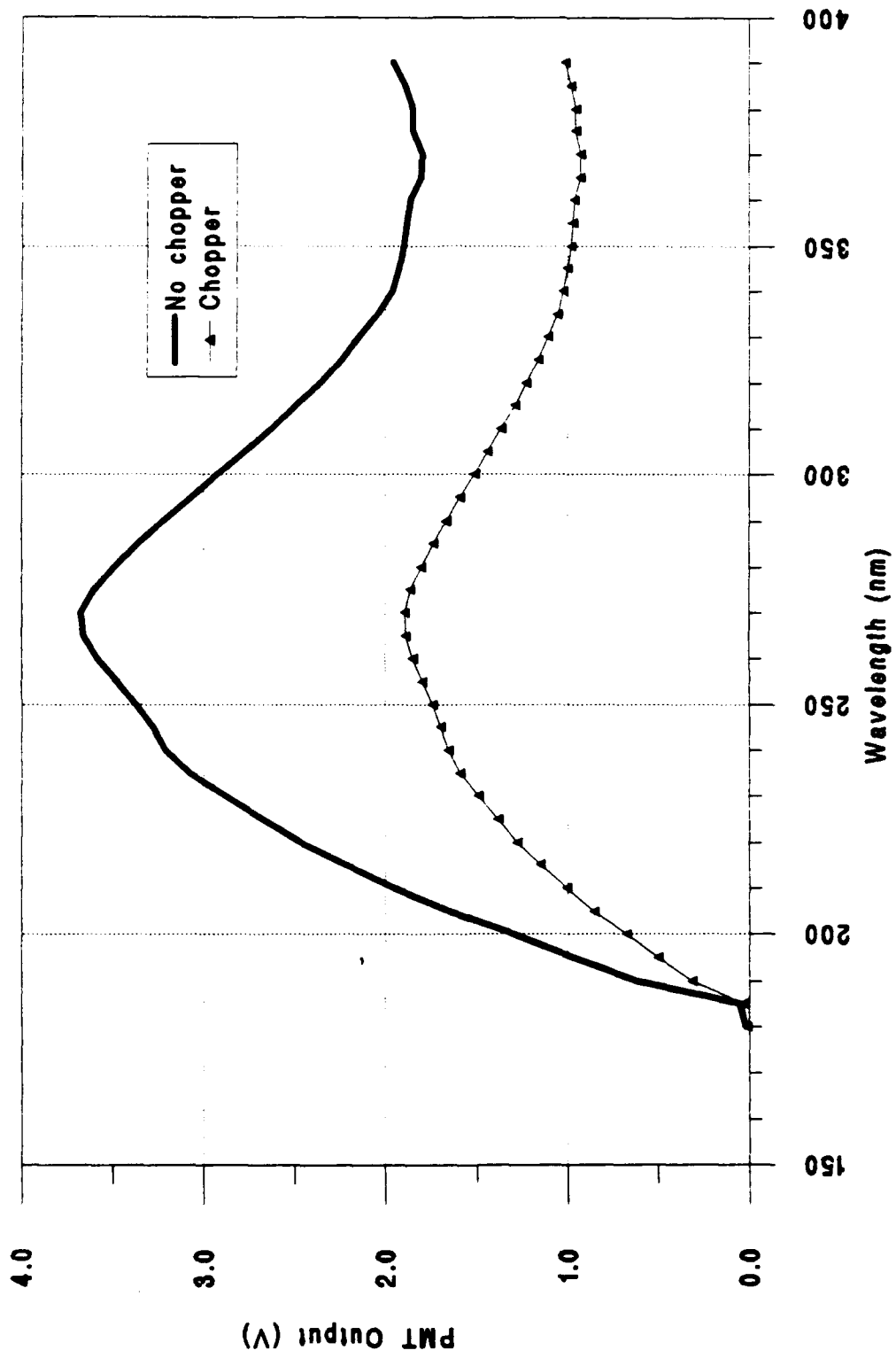


Figure 15 D2 Lamp Spectrum With and Without Light Chopper

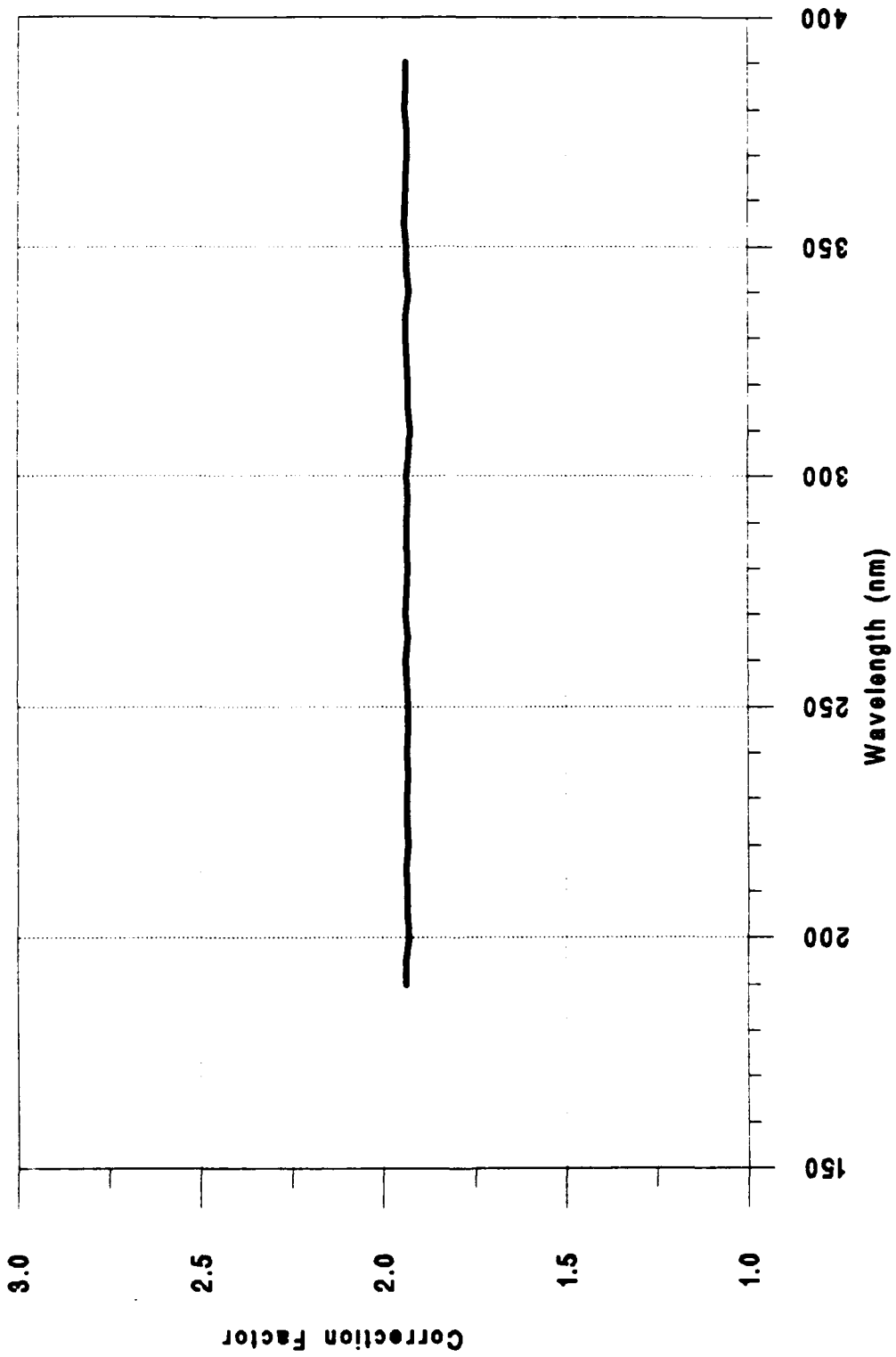


Figure 16 Light Chopper Correction Curve

Since the correction factor is roughly 2, the light chopper removes one half of the light from the D<sub>2</sub> lamp, as would be expected from the duty cycle. The error for this correction is not significant since the signal to noise ratio was high and no measurable run to run deviation was observed.

Two neutral density filters of density (D) 2 and 0.5 were used to lower the D<sub>2</sub> lamp intensity to a level comparable to that of SL. This was necessary so that the output level of the lock-in amplifier could be calibrated at the same sensitivity and time constant settings as those used to record the raw data SL curves. The filters were stacked and placed between the light chopper and the fiber.

Light transmitted through the filters can be estimated by

$$T = 10^{-D} \quad (1)$$

where  $T$  is the transmittance and  $D$  is the sum of the filter density values, or in this case 2.5. The transmittance is therefore 0.0032, or the light is attenuated by a factor of 316.  $T$  represents a nominal transmittance. In actuality the filter response is not flat for all wavelengths in the calibration region. Figures 17 and 18 show the 2D and 0.5D filter responses respectively as measured with a photospectrometer. The photospectrometer values closely match the manufacturers stated response.

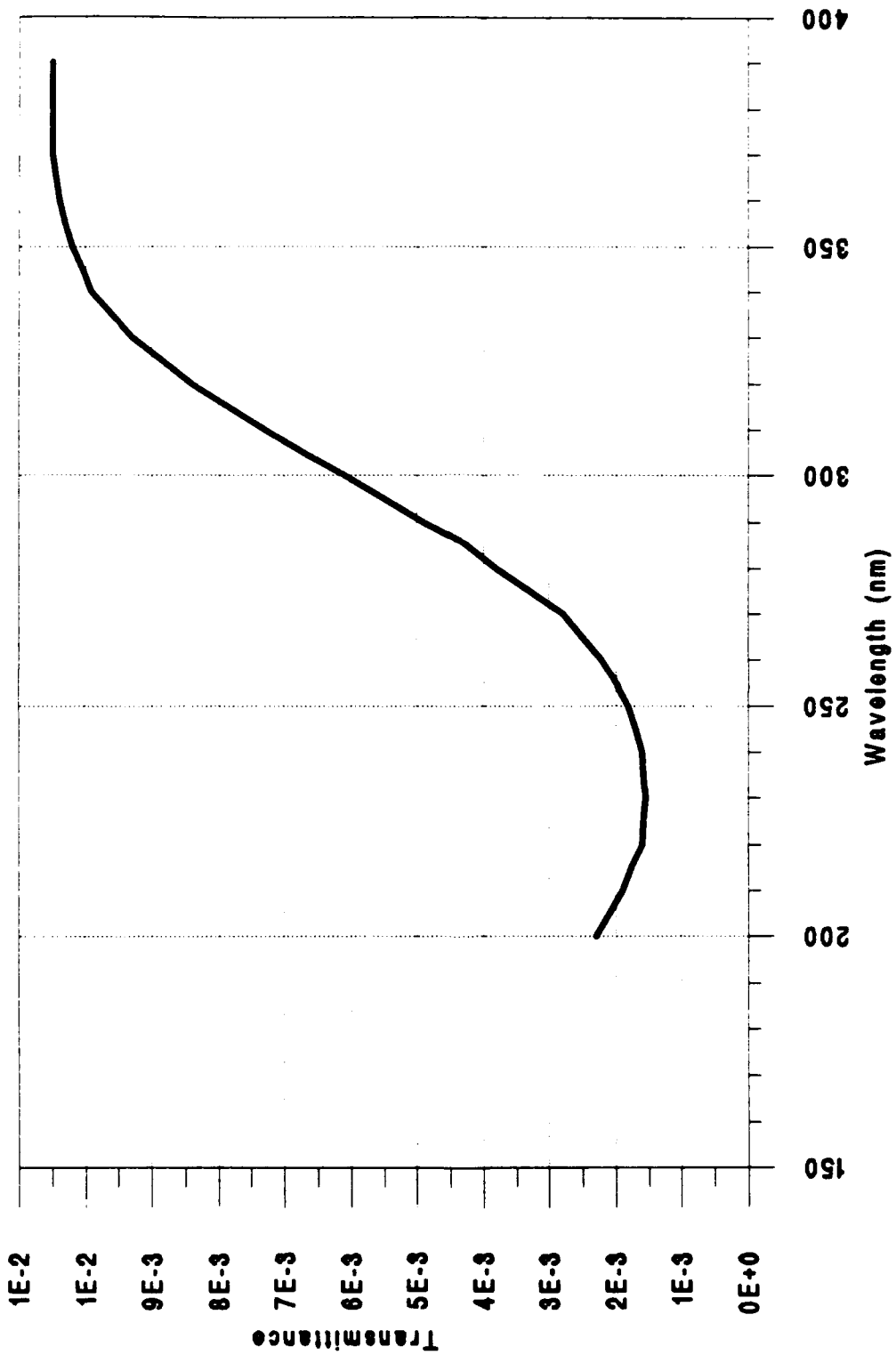


Figure 17 2D Filter Transmission Curve

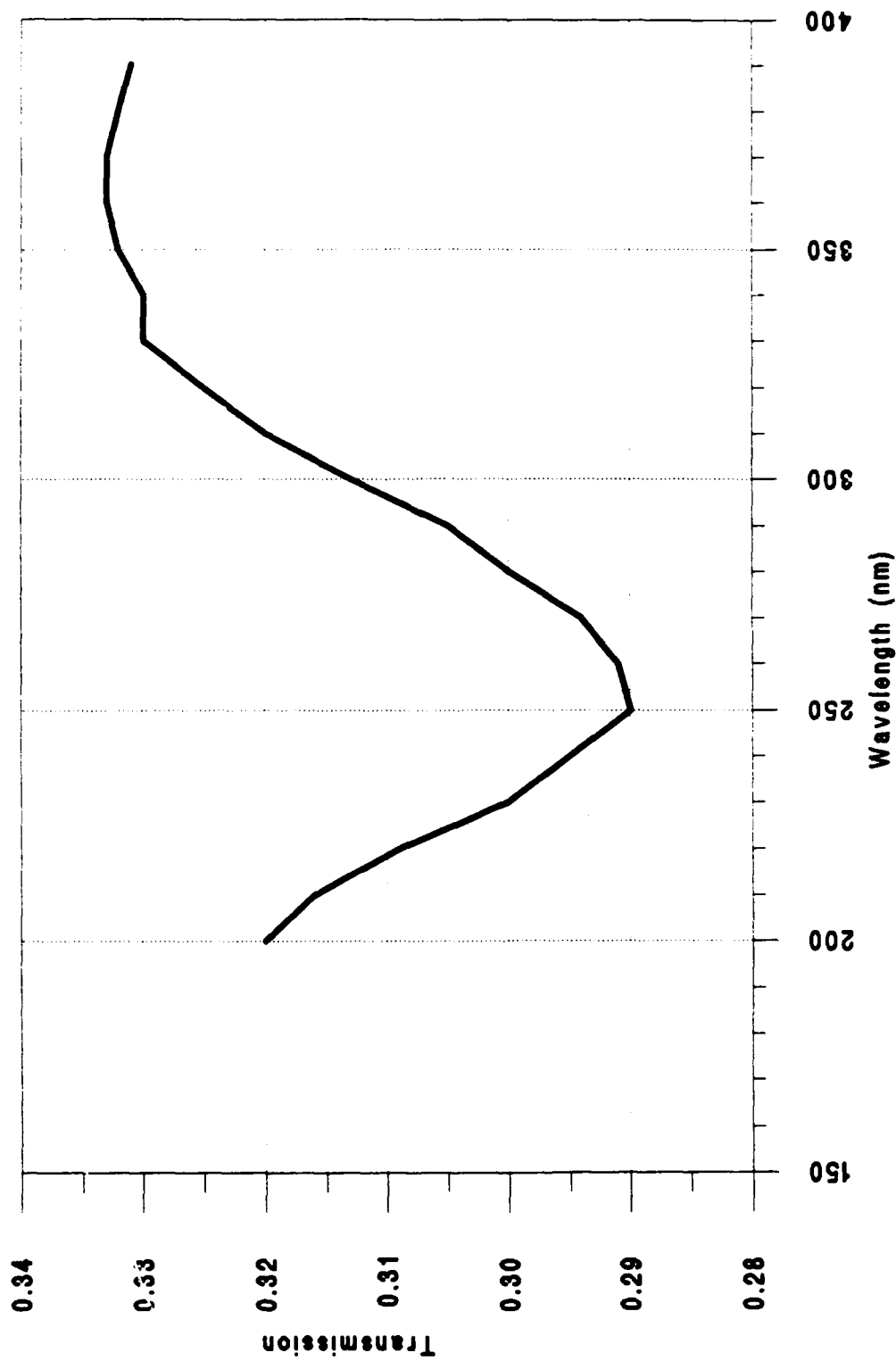


Figure 18 0.5D Filter Transmission Curve

Lock-in amplifier settings identical to those used to collect raw data were then used to view the D<sub>2</sub> lamp spectrum. Figure 19 shows the mean system response of the D<sub>2</sub> lamp, with the light chopper and neutral density filters, for four scans. There is some run to run deviation, as indicated by the error bars. This data was corrected for the effects of the light chopper and the measured filter responses, as stated above, to produce Figure 20, the derived response of the D<sub>2</sub> lamp for the fiber/ spectrometer/ lock-in system. The error bars represent the errors from the run to run deviation in the D<sub>2</sub> spectrum described above.

To obtain the short wavelength correction curve, the D<sub>2</sub> lamp calibration data, Figure 14, was divided by the derived D<sub>2</sub> response curve, Figure 20. The correction curve is shown in Figure 21 with associated error bars. The error in the D<sub>2</sub> calibration data, as stated by the manufacturer, was 1% at most and was ignored. Figure 21 was used to correct the raw data for variations in the system spectral response for the 200 nm to 400 nm wavelength region. The Y axis units of Figure 21 are

$$\frac{\frac{\mu\text{Watts}}{\text{cm}^2 \text{ nm}}}{\text{Lock-In Amp. Output (V)}}$$

When raw data curves are multiplied by Figure 21, the

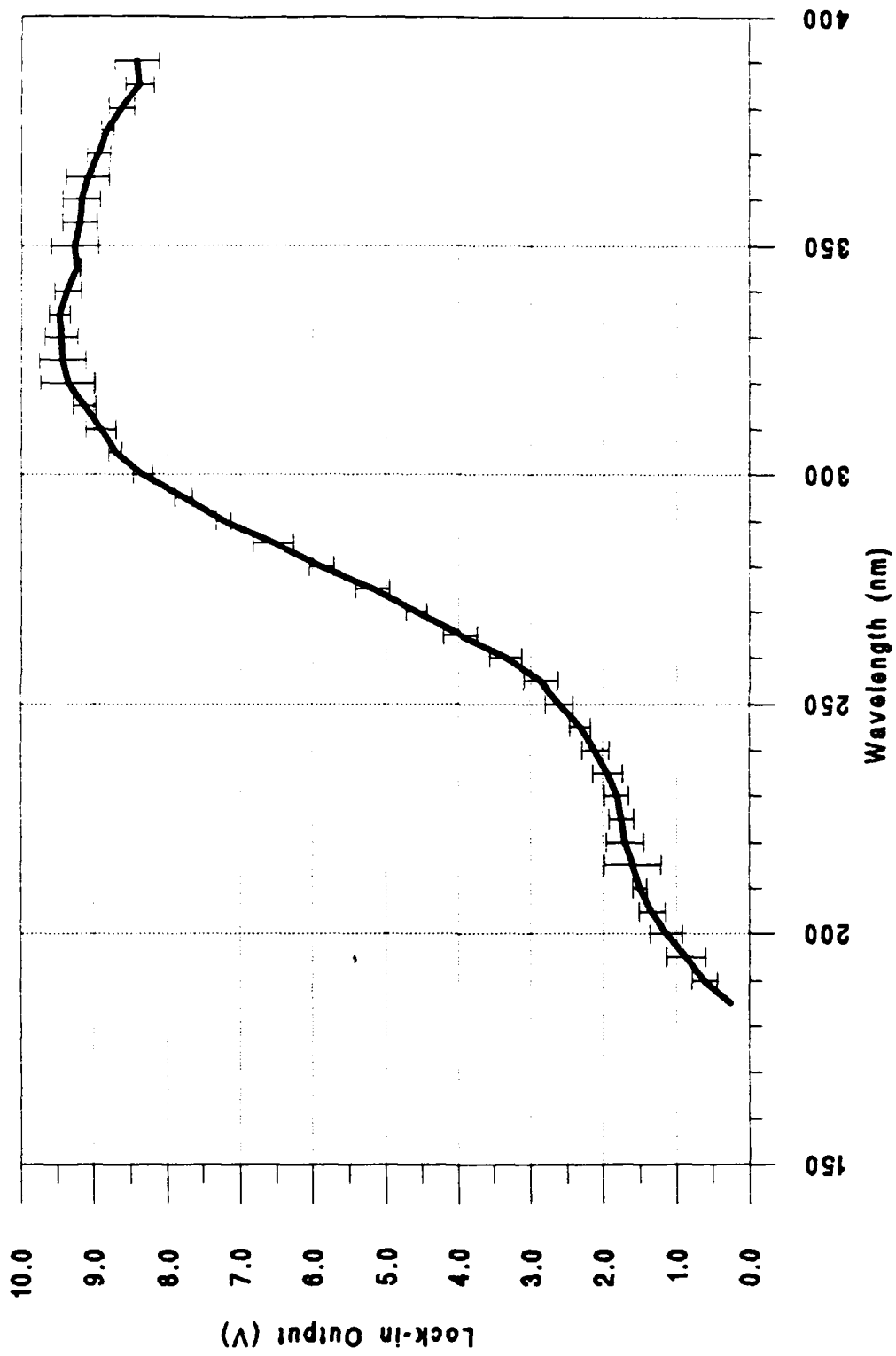


Figure 19 Mean System Response to D2 Lamp

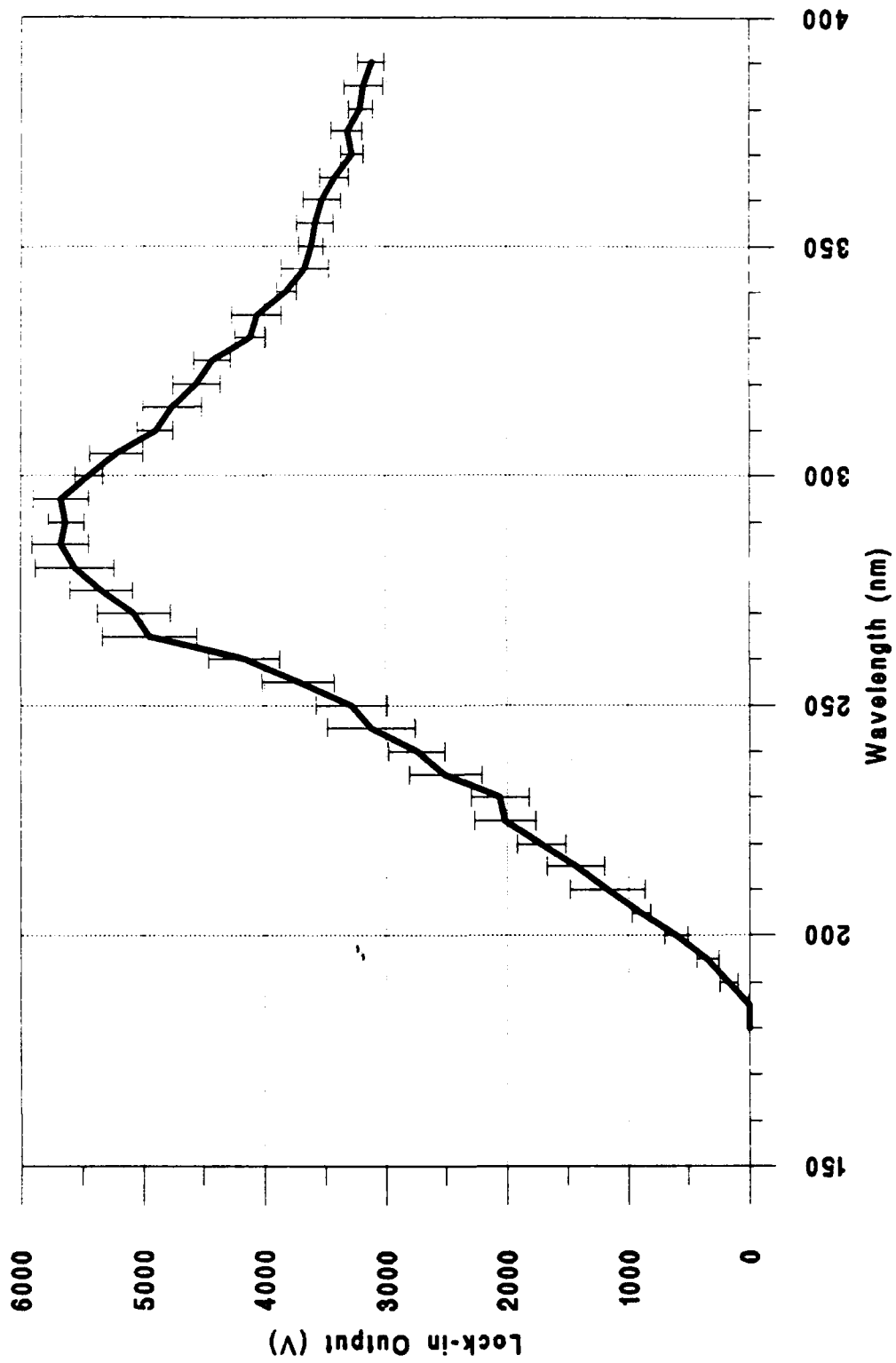


Figure 20 Derived System Response to D2 Lamp

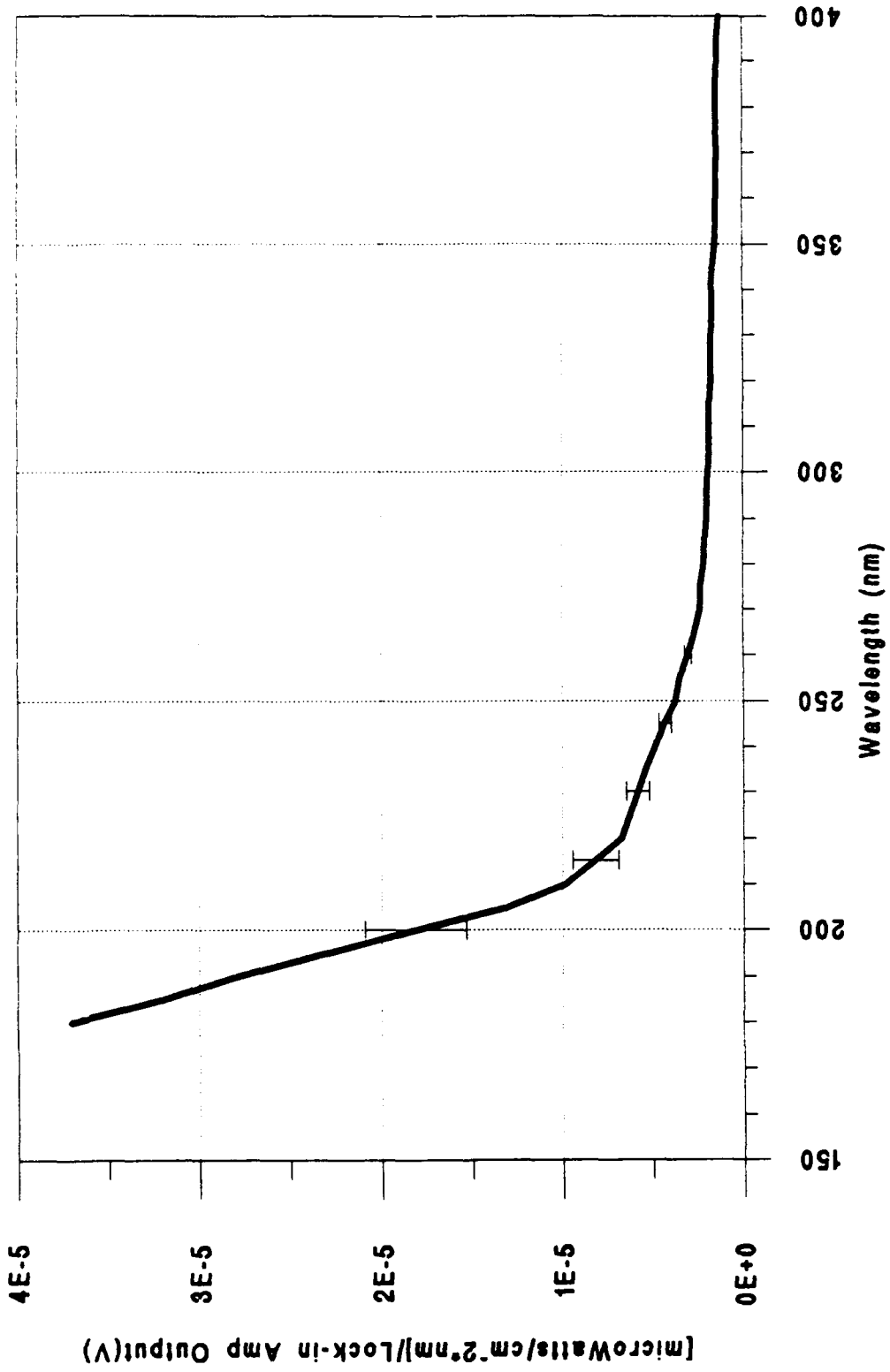


Figure 21 D2 Lamp Correction Curve

resulting spectra will have absolute Y axis units of  $\mu\text{Watts}/\text{cm}^2 \cdot \text{nm}$  .

### 3. Long Wavelength Calibration

A Tungsten-Halogen (TH) lamp was used to determine the system spectral response in the wavelength region 300 nm to 750 nm. Figure 22 shows the calibration curve for the lamp as provided by the manufacturer. Figure 23 shows the TH lamp spectrum through the fiber/spectrometer system, excluding the lock-in amplifier. There was no measurable run to run deviation of the recorded TH lamp spectra. Figure 22 was divided by Figure 23 to produce Figure 24, a spectral response correction curve for the long wavelength region. The Y axis units in this case are in relative output power units, since the light chopper and lock-in amplifier were not used for an absolute calibration. The error in the manufacturers calibration data for the TH lamp was on the order of 1%, and was ignored. Therefore, there were no error bars in the long wavelength correction curve, Figure 24.

### 4. System Calibration Curve

Figure 21, the short wavelength correction curve, and Figure 24, the long wavelength correction curve, were combined to produce a system calibration curve. Figure 25 shows Figures 21 and 24 plotted together. The long wavelength curve has been multiplied by a scaling factor of  $5.9 \times 10^{-5}$  to match the short wavelength curve amplitude, since the short

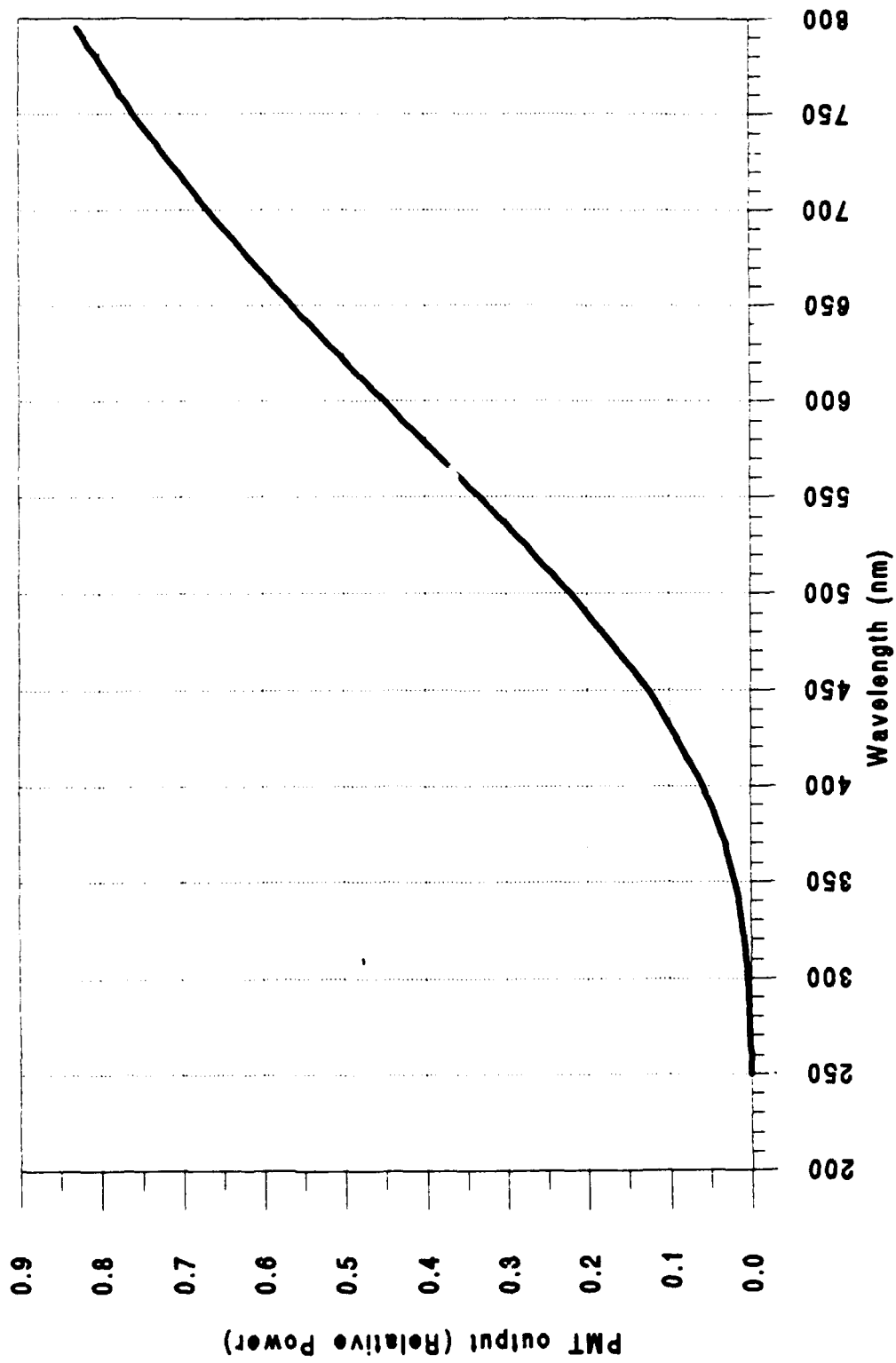


Figure 22 Manufacturers Calibration Data for Tungsten-Halogen Lamp

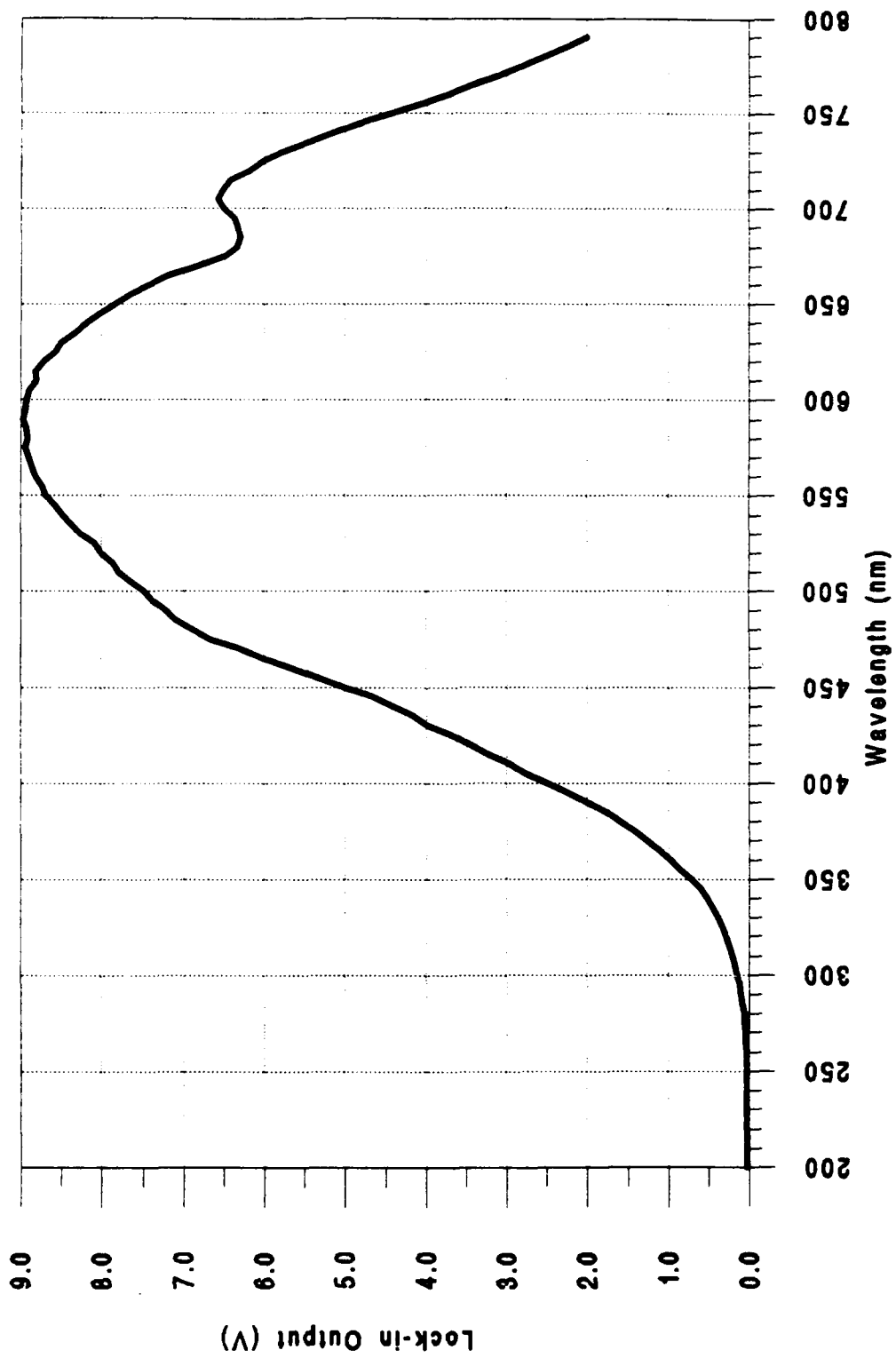


Figure 23 Tungsten-Halogen Lamp - System Spectrum

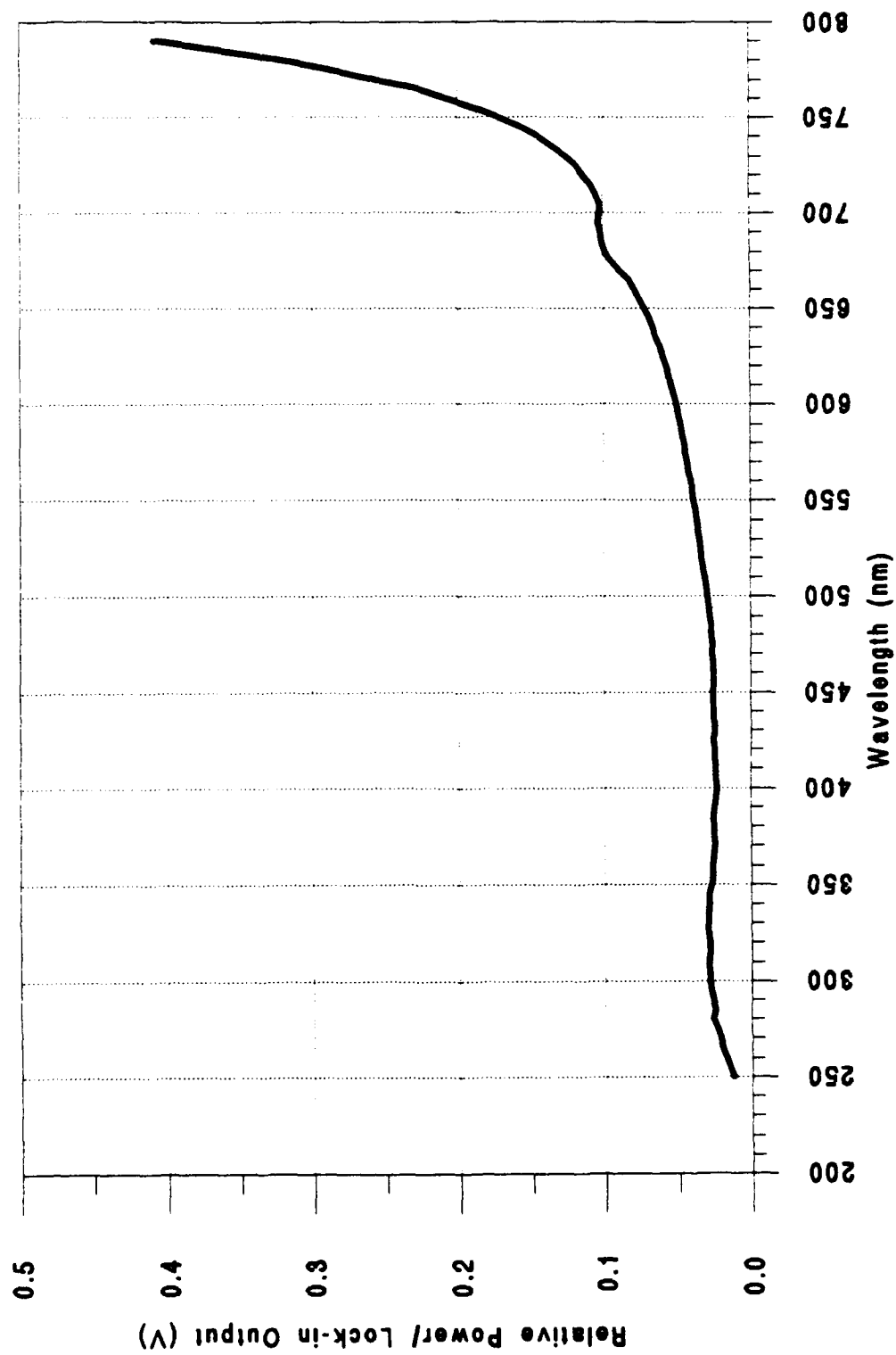


Figure 24 Tungsten-Halogen Correction Curve

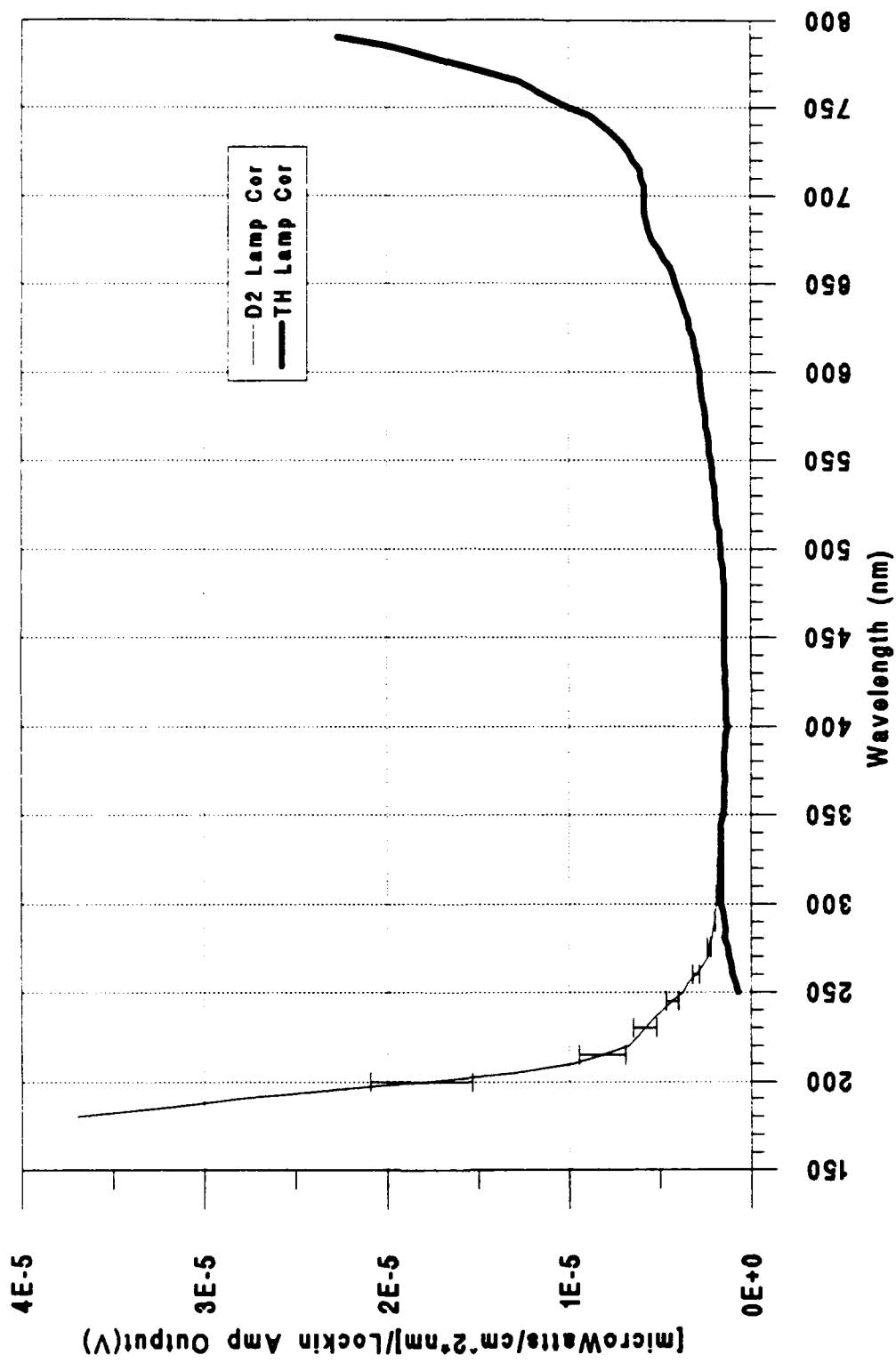


Figure 25 D2 and Tungsten-Halogen Correction Curves

wavelength curve contains absolute power units. The curves overlap nicely in the region from 360 nm to 400 nm. Figure 26 was produced by joining the short and long wavelength calibration curves at 360 nm. This is the system spectral correction curve which, when multiplied by raw data spectra, will correct the raw data for system response variations to give a true, absolute power spectrum. Error bars in Figure 26 indicate the error associated with the D<sub>2</sub> lamp calibration procedure.

#### 5. UV Transmission in Water and 25% Glycerin Solution

The transmission of light through water and a 25% glycerin solution was measured with a photospectrometer to determine how the SL spectra might be affected by UV absorption in the liquids. The transmission was measured through a 1 cm sample of each liquid. Figure 27 shows the result of the photospectrometer measurement.

SL raw data was recorded through the fiber at a distance of about 0.5 cm from the source. At 0.5 cm the transmission of light from the SL source is greater than that indicated in Figure 27. For water, the absorption of UV light at the system calibration limit (200 nm) was negligible. For the 25% glycerin solution, the absorption of UV light was negligible above 220 nm. Since very little light was observed at 200 nm, as indicated in Figure 11, the correction for absorption by the glycerin solution would be small and well

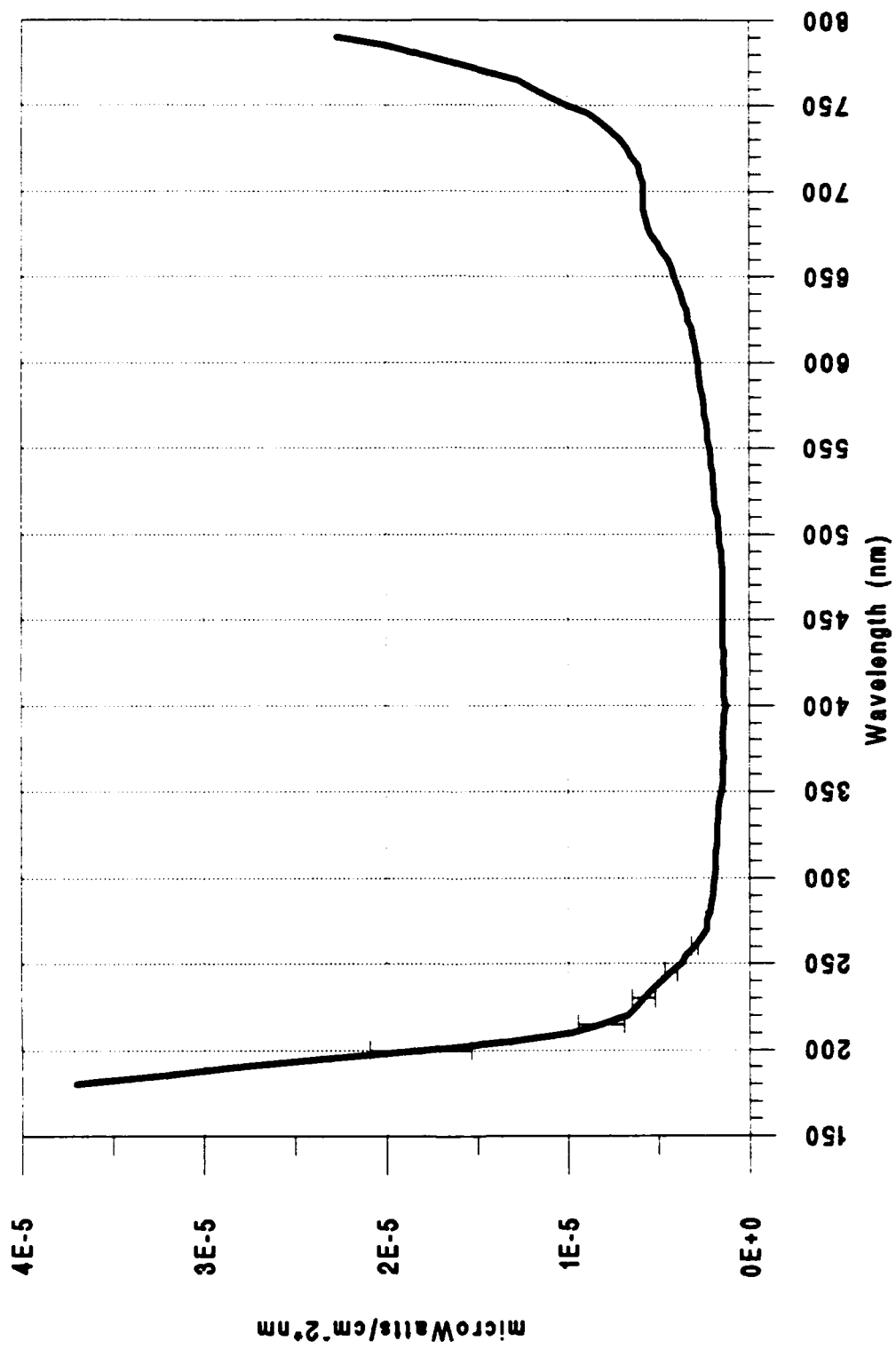


Figure 26 System Spectral Correction Curve

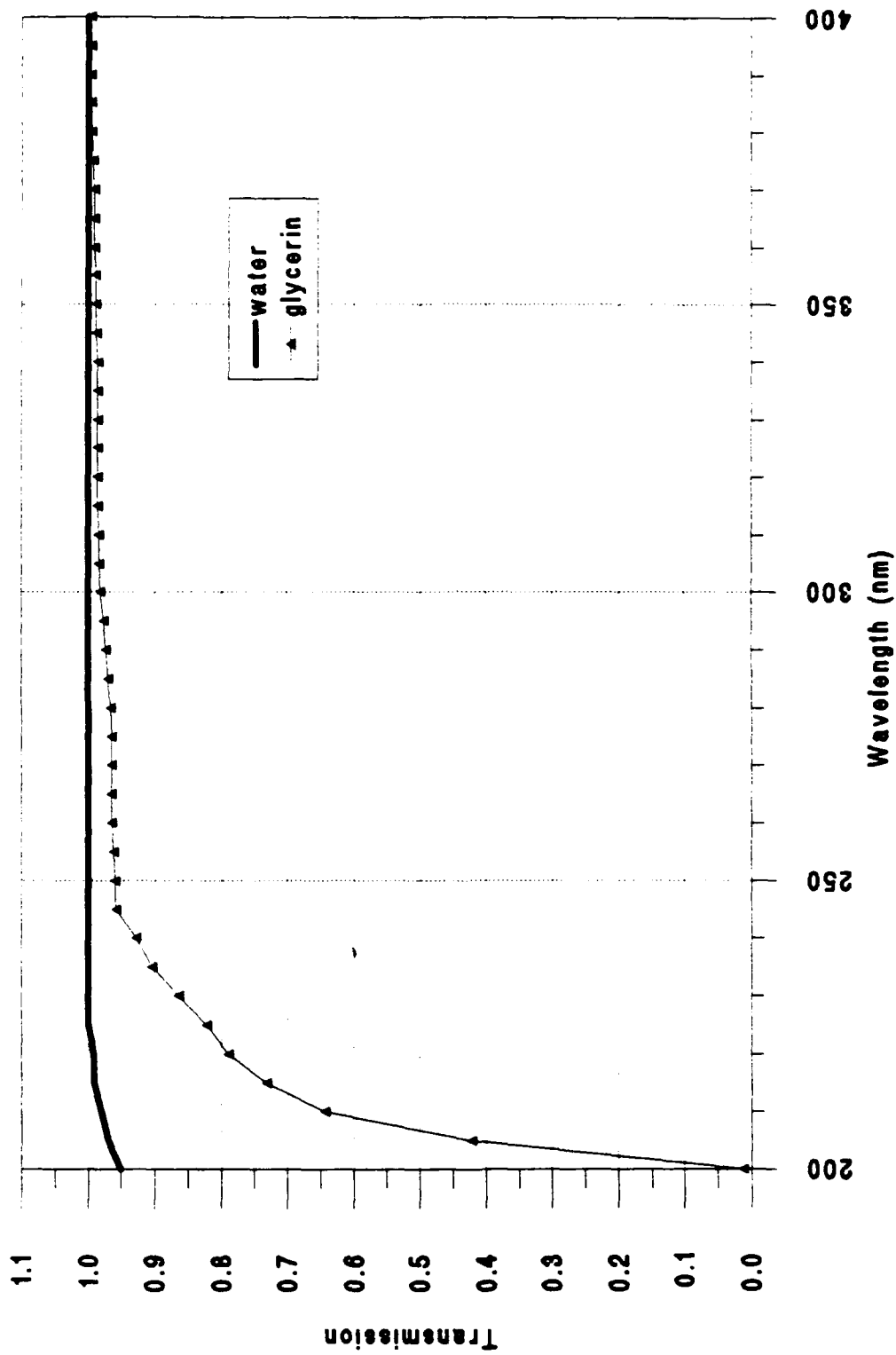


Figure 27 UV Transmission Through 1cm Water and 25% Glycerin Solution

within the error introduced by the system spectral correction curve, Figure 26. Therefore no corrections were made for the absorption of UV light by the liquids.

#### IV. DATA ANALYSIS

##### A. BACKGROUND

The measured raw data spectra will be analyzed for common characteristics and observed differences among the various solutions.

Figure 26, the system spectral correction curve, was used to correct the SL raw data spectra for component spectral response characteristics. To obtain a true SL spectra in absolute power units, a correction was also required for the fiber distance from the SL source and for the SL duty cycle. These corrections are discussed and individual corrected spectra are presented for SL in water and two water/glycerin mixtures.

A comparison will be made between the corrected SL spectrum in water and the corrected water/glycerin spectra to reveal significant differences. A comparison is made between the corrected SL spectrum in water and an SL spectrum in water produced by Putterman. The water and water/glycerin spectra are also compared to spectra determined by Carlson to reveal significant similarities.

The SL spectra are then modeled by a blackbody radiation distribution. The model predicts an effective peak temperature and size if SL were characterized by blackbody

radiation. The SL effective temperature and size are compared to existing theoretical and experimental values.

#### **B. ANALYSIS OF RAW DATA SPECTRA**

The raw data spectra developed above in Figures 8, 10, and 12 contain an observed similarity. Each raw data set indicates a relatively large run to run intensity fluctuation. However, the normalized curves indicate that the run to run shape of the spectra are consistent within each fluid type. The consistent shape indicates that the spectra are the same for large variations in run to run intensity over long run time periods (i.e., minutes). The intensity fluctuations were due to run to run adjustments in the driving force. The consistency of the spectra shape with large variations in intensity agrees with experimental conclusions presented by Putterman [Ref. 6 p.1183].

Several differences were observed in the raw data spectra. The mean peak intensity decreases with an increase in glycerin concentration. All solutions were driven at nearly the same amplifier settings. However, the frequency at which SL was achieved increased with the increase in glycerin concentration (Table 1). The frequency increase is due to the fact that the speed of sound in glycerin ( $\sim 2000$  m/s) is greater than that in water ( $\sim 1500$  m/s). The increased driving frequency may equate to a decrease in the driving signal force on the bubble

thereby decreasing the SL intensity for greater concentrations of glycerin. The driving signal forces on the bubble for the various solutions need to be measured to determine a definite trend in the driving signal force on the bubble, as it may determine the SL intensity in the various solutions.

The peak in the normalized raw data sets are located at different wavelengths, depending on the solution type. The water spectrum peak is at 300 nm and appears sharper than the two glycerin solutions. The glycerin solutions peak at about 350 nm and are broad and not well defined. The effect of the variation in the location of the peak signal for the different solutions will become apparent when the spectra are corrected.

The water spectrum, Figure 8, produces more light in the UV region than the glycerin spectra. The amount of light at 200 nm for the water spectrum is roughly 10% of the peak intensity. The two glycerin spectra have almost no light at 200 nm. The fall off of all the spectra as 200 nm is approached, including Figure 20 the D<sub>2</sub> lamp spectrum (which in actuality peaks at 200 nm), is due to the fall off in the system spectral response. It appears that SL in water is producing more UV light. Again, this fact will become more apparent in the corrected spectra.

## C. CORRECTED SL SPECTRA

### 1. Corrected Water Spectrum

Figure 28, the corrected SL spectrum in water, was produced by multiplying the mean water spectrum in Figure 8 by the system spectral correction curve in Figure 26. The error indicated in Figure 28 is the error derived from the calibration error in Figure 26 and the error in the shape of the normalized raw data water spectrum, Figure 9.

The Y axis units of Figure 28 indicate the average power radiated per area per wavelength interval by SL at a distance of 0.5 cm from the source (the distance from the fiber to the source). To obtain the total power radiated at the source per wavelength interval, the data was corrected for the 0.5 cm distance. To correct for the 0.5 cm distance, the data was multiplied by the surface area of a sphere of radius 0.5 cm, or  $4\pi(0.5 \text{ cm})^2 = \pi \text{ cm}^2$ . The Y axis units now become  $\mu\text{Watts/nm}$ , or average power radiated per wavelength interval at the source, assuming SL radiates equally in all directions. Figure 29 shows the average power output per wavelength interval for SL in water.

The water spectrum was calibrated with two continuous output lamps. Figure 29, the average power output, can then be corrected for the duty ratio between the calibration lamps and SL to produce the total power output per SL flash. The SL flashes occur 43,000 times per second, and assuming a flash

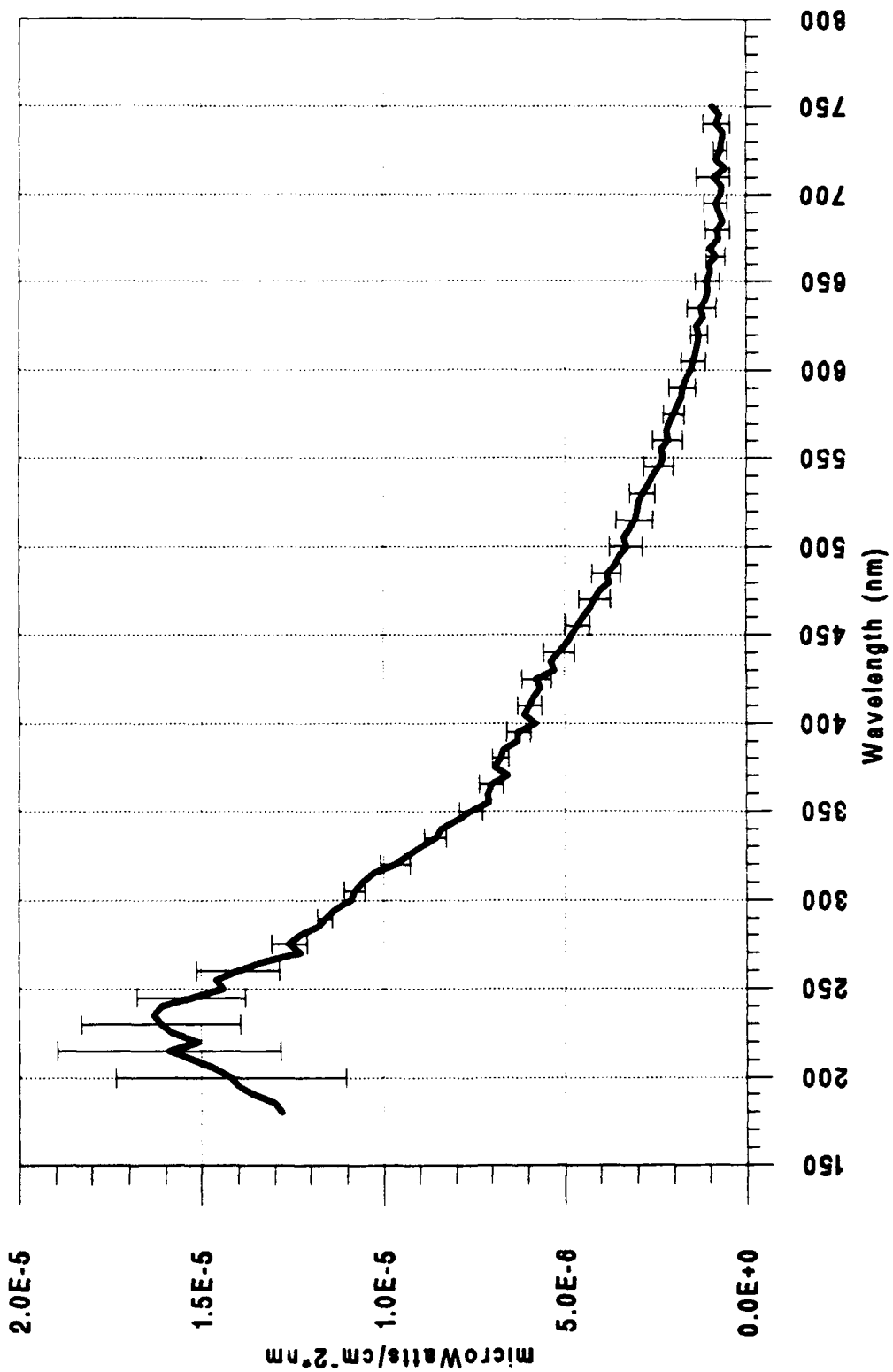


Figure 28 Corrected SL Spectrum in Water

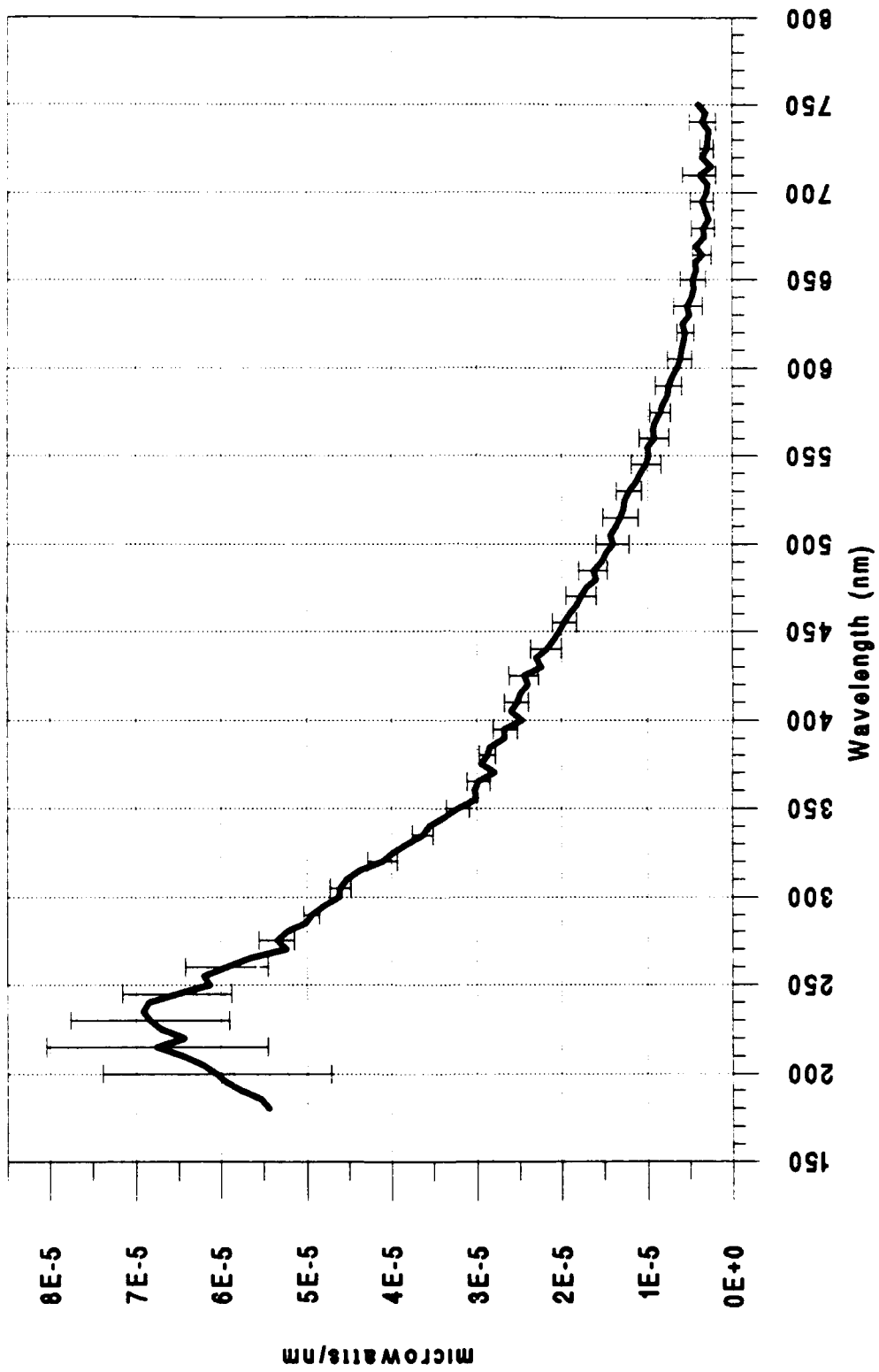


Figure 29 Average Power from SL in Water

pulse width of 50 ps, the SL source is only radiating 2.15  $\mu$ s for every second the calibration sources radiate. Therefore Figure 29 was multiplied by a duty ratio of  $1 \text{ s}/2.15 \mu\text{s} = 4 \times 10^5$  to obtain the power radiated during a single SL flash. Figure 30 shows the resulting spectrum.

### **2. Corrected 25% Glycerin Spectrum**

The raw data 25% glycerin spectrum, Figure 10, was multiplied by the system spectral correction curve, Figure 26, to correct for system spectral response deviations. The resulting spectrum was then multiplied by  $4\pi(0.5 \text{ cm})^2 = \pi \text{ cm}^2$ , to correct for the fiber distance from the source. The corrected 25% glycerin spectrum is shown in Figure 31, indicating the average power output per wavelength interval. The error bars indicate the sum of the calibration error and the error in the shape of the 25% glycerin raw data curve.

To determine the power radiated during a single SL flash at a frequency of 46 kHz for the 25% glycerin solution, the data was multiplied by the duty ratio of  $1 \text{ s}/2.3 \mu\text{s} = 4.3 \times 10^5$ . Figure 32 shows the power radiated during a single SL flash for the 25% glycerin solution.

### **3. Corrected 40% Glycerin Spectrum**

The raw data 40% glycerin spectrum, Figure 12, was multiplied by the system spectral correction curve Figure 26, to correct for system spectral response deviations. The resulting spectrum was then multiplied by  $4\pi(0.3 \text{ cm})^2 = 1.13$

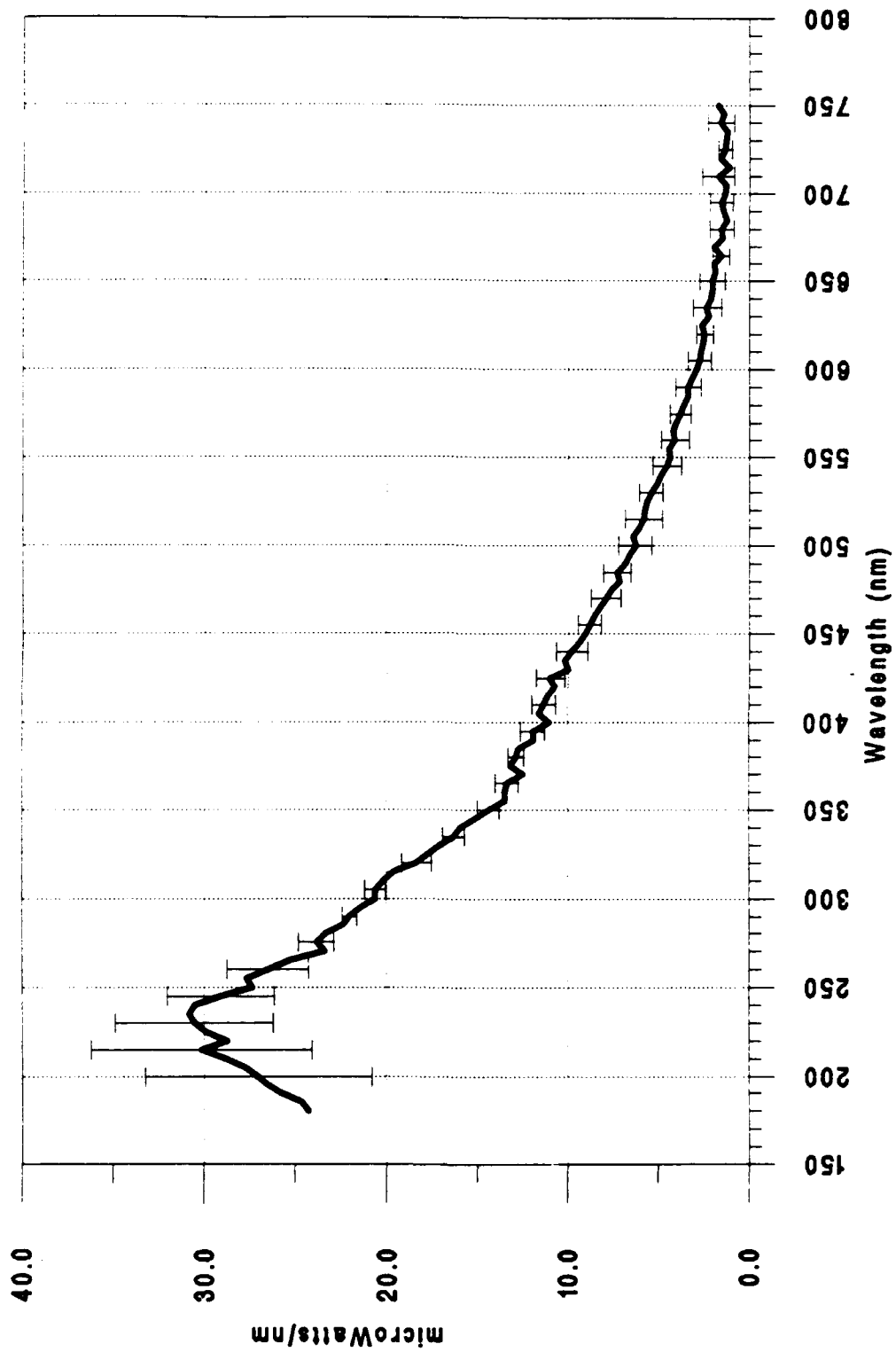


Figure 30 Power Radiated in a Single Flash for SL in Water

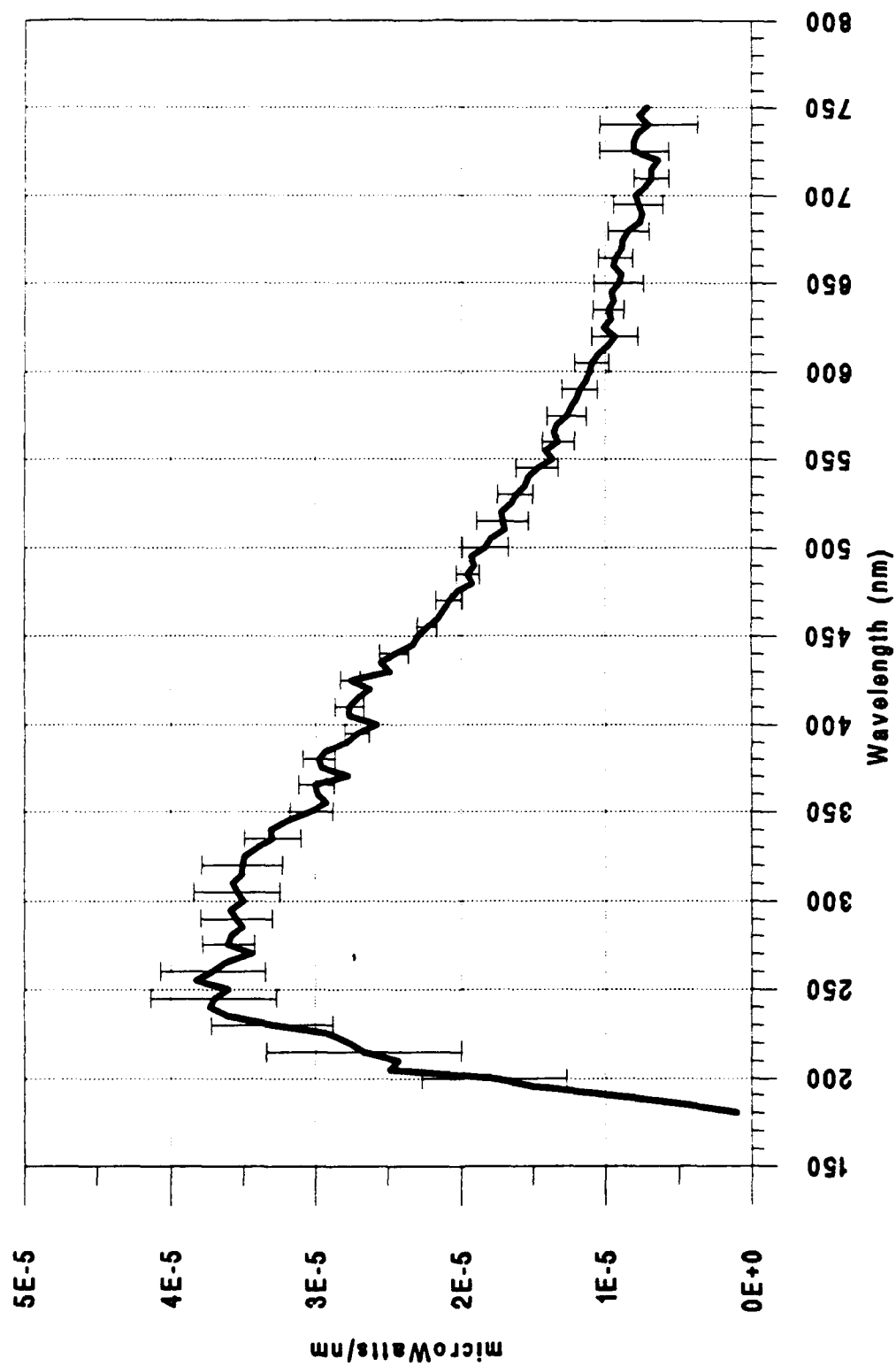


Figure 31 Corrected SL Spectrum in 25% Glycerin Solution

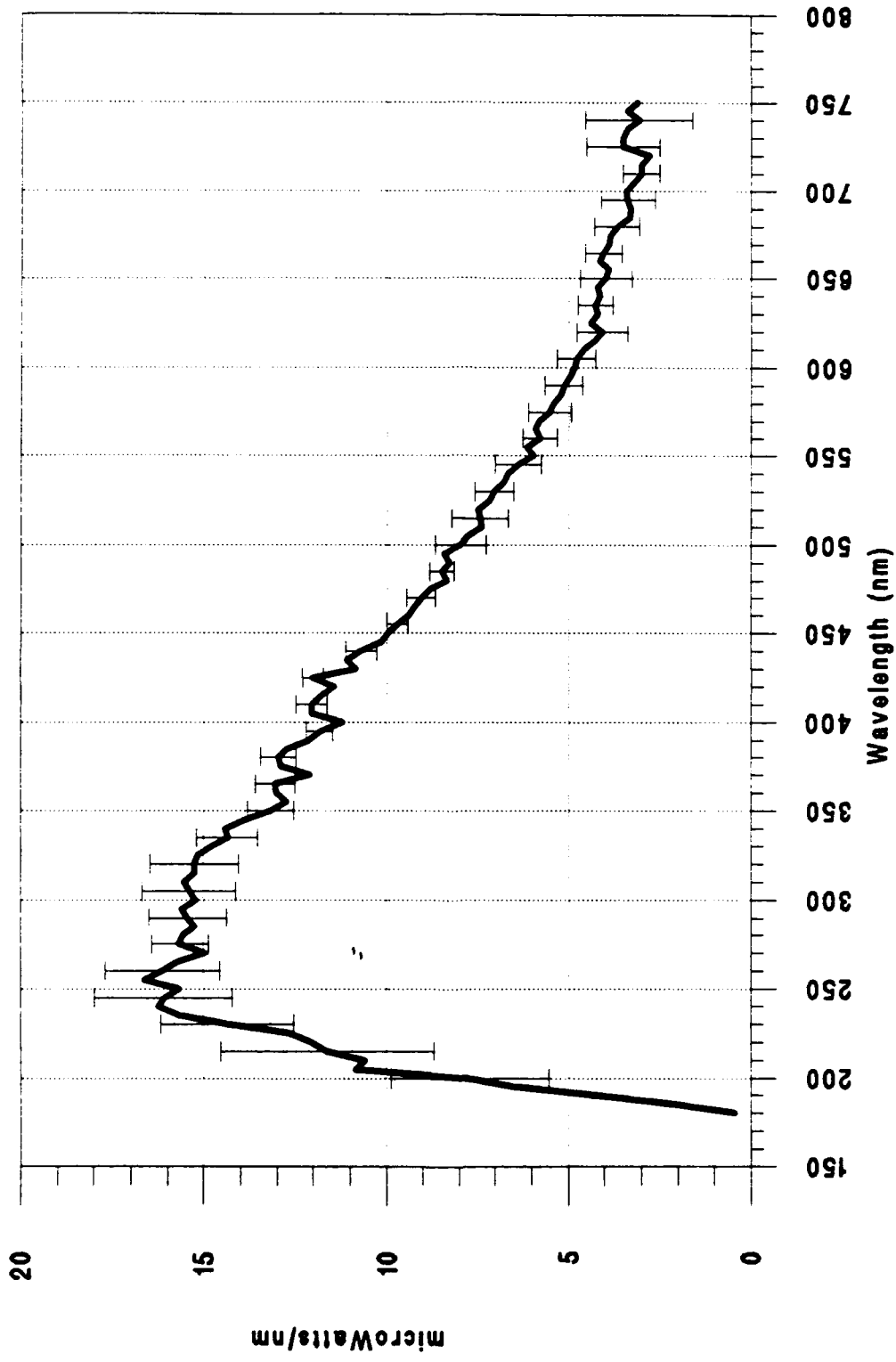


Figure 32 Power Radiated in a Single Flash for SL in 25% Glycerin Solution

$\text{cm}^2$ , to correct for the fiber distance from the source. The corrected 40% glycerin spectrum is shown in Figure 33, indicating the average power output per wavelength interval. The error bars indicate the sum of the calibration error and the error in the shape of the 40% glycerin raw data curve.

To determine the power radiated during a single SL flash at a frequency of 52 kHz for the 40% glycerin solution, the data is again multiplied by the duty ratio, or  $1 \text{ s}/2.6 \mu\text{s} = 3.8 \times 10^5$ . Figure 34 shows the power radiated during a single SL flash for the 40% glycerin solution.

#### D. COMPARISON OF CORRECTED SPECTRA

The corrected SL spectra were compared. Several trends were revealed. Figure 35 shows the three corrected spectra plotted together. The water spectrum shows a greater overall intensity, especially as the system wavelength calibration limit (200 nm) is approached. The water spectrum seems to be peaking at around 230 nm, although it is difficult to say if this is the peak, since the errors are large here.

The 25% glycerin spectrum peak is only half as intense as the water spectrum and occurs around 260 nm. The spectrum is decreasing in intensity as the system wavelength calibration limit is approached. The 25% glycerin spectrum also shows a greater intensity in the visible region of the spectrum as compared to water. SL in 25% glycerin does appear brighter to

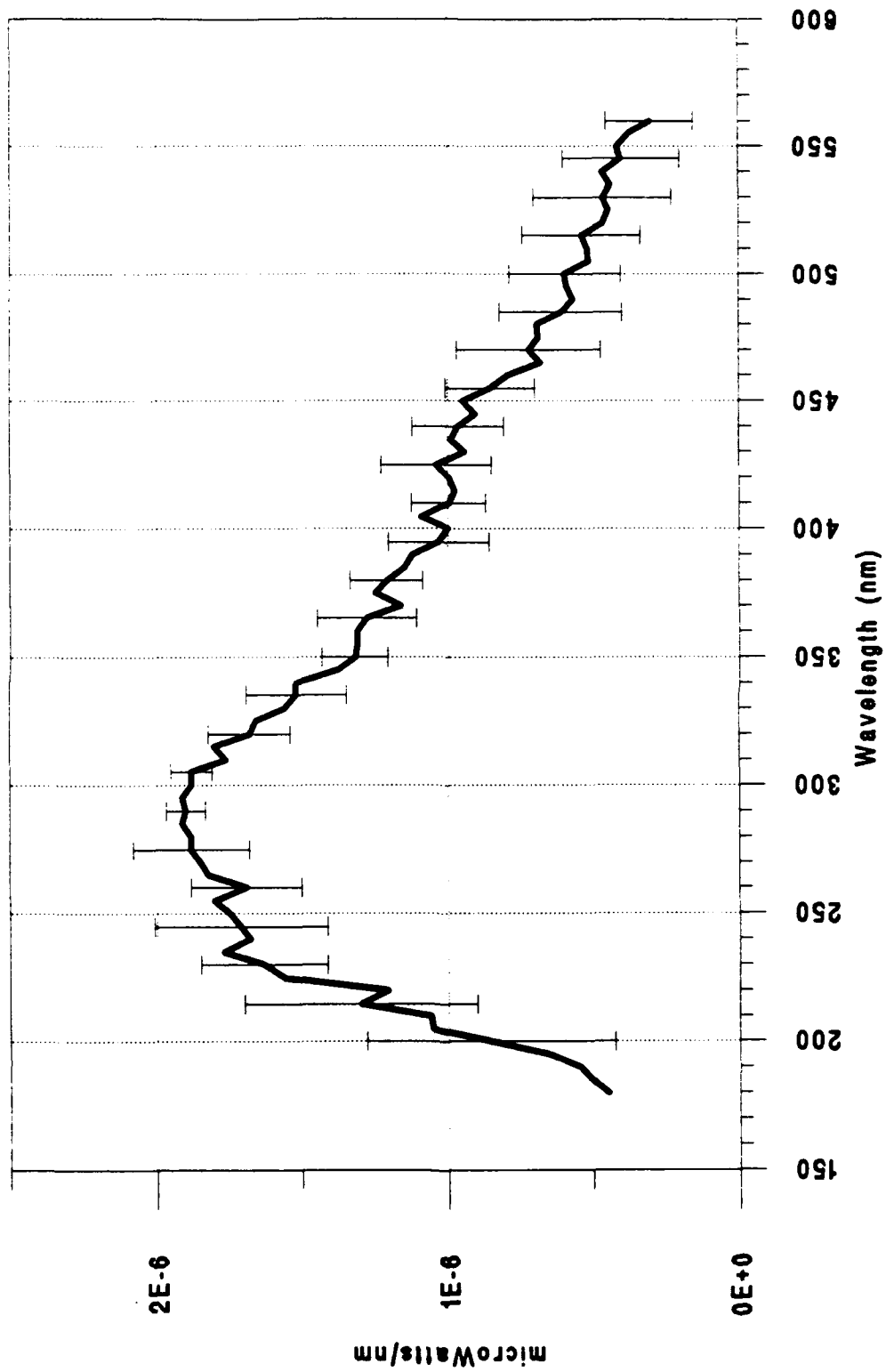


Figure 33 Corrected SL Spectrum in 40% Glycerin Solution

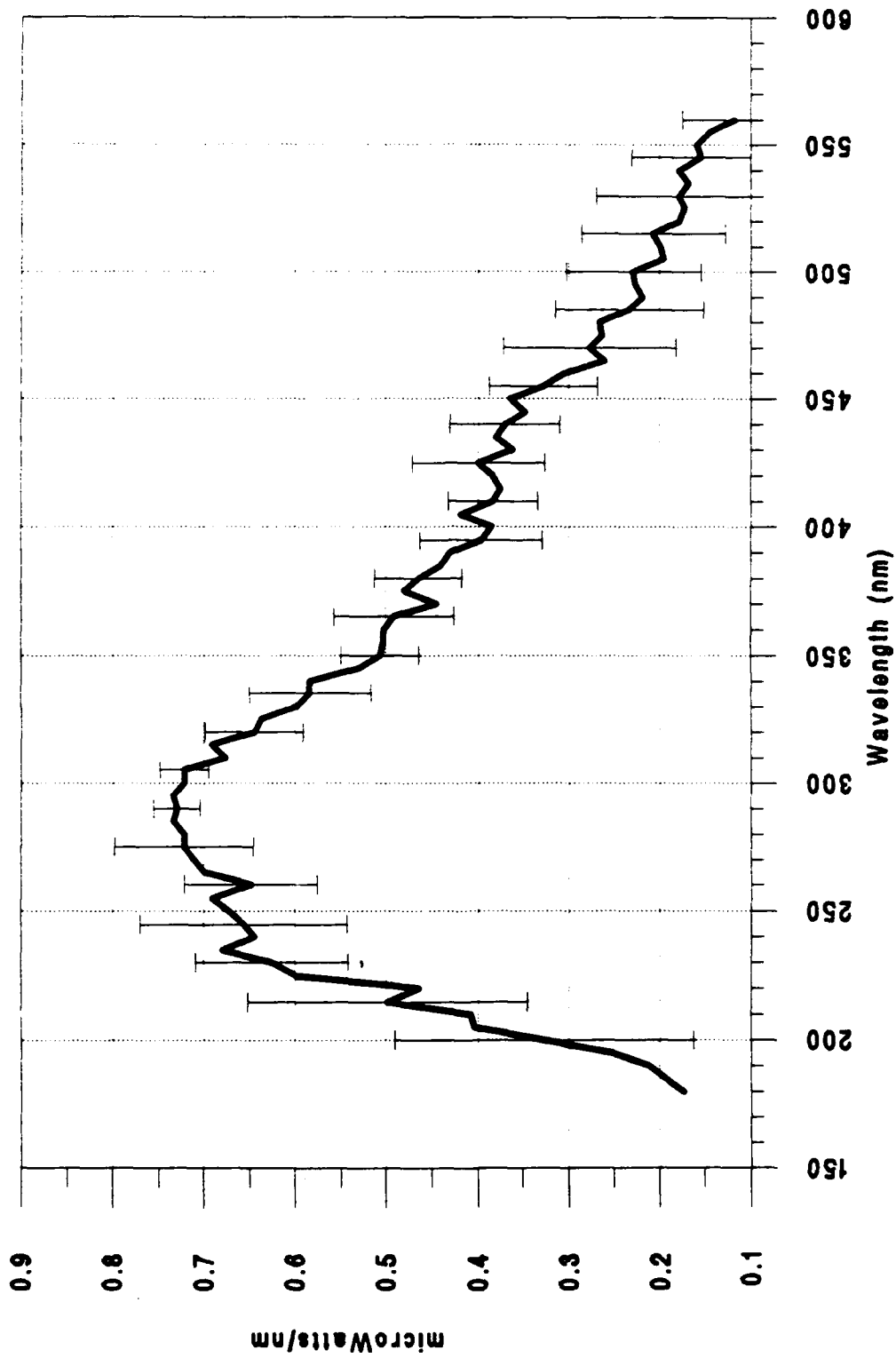


Figure 34 Power Radiated in a Single Flash for SL in 40% Glycerin Solution

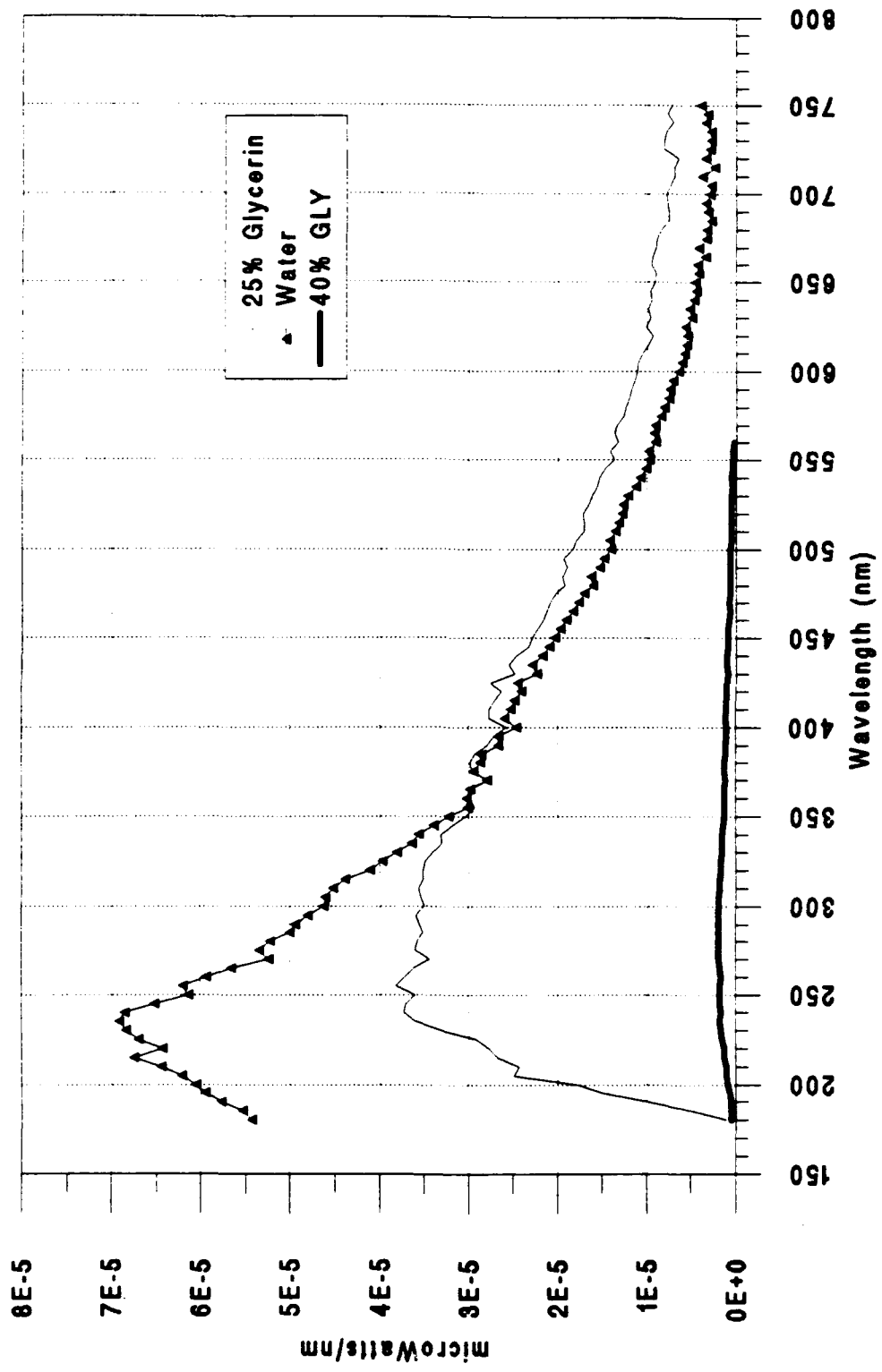


Figure 35 Comparison of SL in Water, 25% Glycerin, and 40% Glycerin Solutions

the eye than SL in water. However, SL in water is much more intense in the UV region.

The 40% glycerin peak is barely visible in Figure 35. Figure 36 shows the three spectra on a semi-log plot. The 40% spectrum peaks around 300 nm and is much less intense than the other two spectra. The 40% spectrum was also decreasing in intensity as the system calibration limit was approached. SL in 40% glycerin was very dim to the eye.

Figure 35 and 36 indicate a decrease in the SL peak intensity with an increase in glycerin concentration. The wavelength of the peak intensity drifts to longer wavelengths as the glycerin concentration is increased. Recall that the frequency of the driving signal required to achieve SL in each of the various solutions was increasing with an increase in glycerin concentration. Therefore, increasing the glycerin concentration has two physical effects on SL:

1. Decreases the peak intensity of SL.
2. Shifts the spectrum peak to longer wavelengths.

More work is necessary to determine just how the strength of the sound field at the bubble position is affected by changing the frequency and the glycerin concentration, since the strength of the sound field greatly influences the SL intensity and possibly the spectral characteristics.

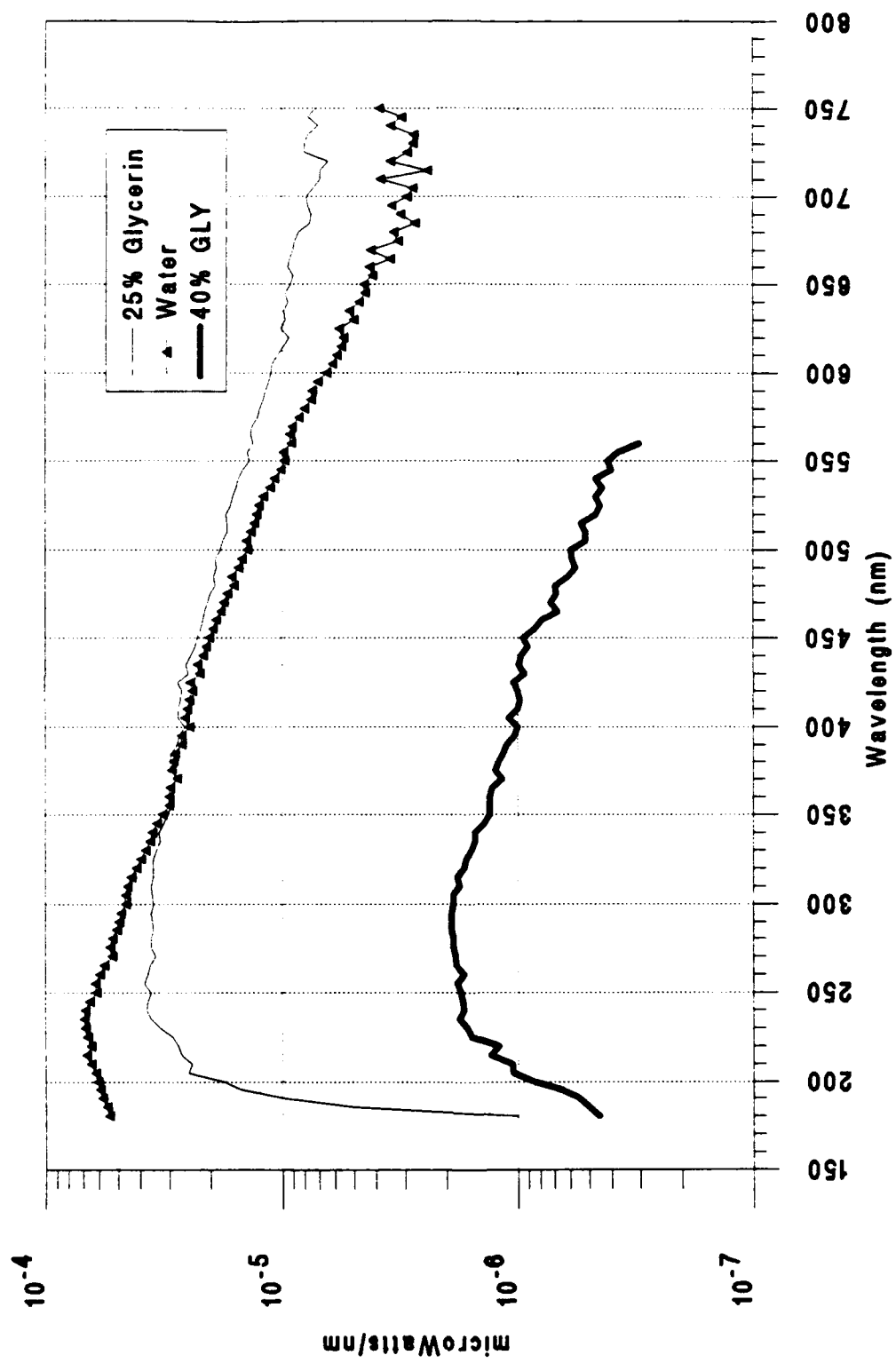


Figure 36 Comparison of SL in Water, 25% Glycerin, and 40% Glycerin Solutions

#### **E. COMPARISON OF SL IN WATER - NPS vs UCLA**

A spectrum was produced by Putterman at UCLA, in water [Ref 6]. Figure 37 shows the UCLA spectrum plotted with Figure 29, the average power radiated by SL in water. The spectra are relatively similar and peak at the same place with nearly the same radiating power. The UCLA spectrum was calibrated with only a deuterium lamp, which is not a smooth continuous source at wavelengths longer than 400 nm. This may account for the discrepancy between the spectra at wavelengths between 300 nm and 600 nm.

The NPS spectrum indicates more light at 200 nm as compared to the UCLA spectrum (Figure 37). The increased sensitivity in the 200 nm region is probably due to a higher PMT, grating, and/or better fiber response by the NPS system.

#### **F. SL SPECTRA MODELED BY A BLACKBODY RADIATION DISTRIBUTION**

The physical mechanism that produces SL radiation is currently unexplained. The spectra produced by SL are fairly smooth and continuous with no evidence of spectral lines. There is evidence of a peak in the spectra followed by a relatively long tail. Therefore it is natural to attempt to compare the SL spectra with other known characteristic spectra that occur in nature. A blackbody spectrum represents a smooth, continuous radiation distribution, with a defined peak and a long tail. The blackbody spectrum is a function of the

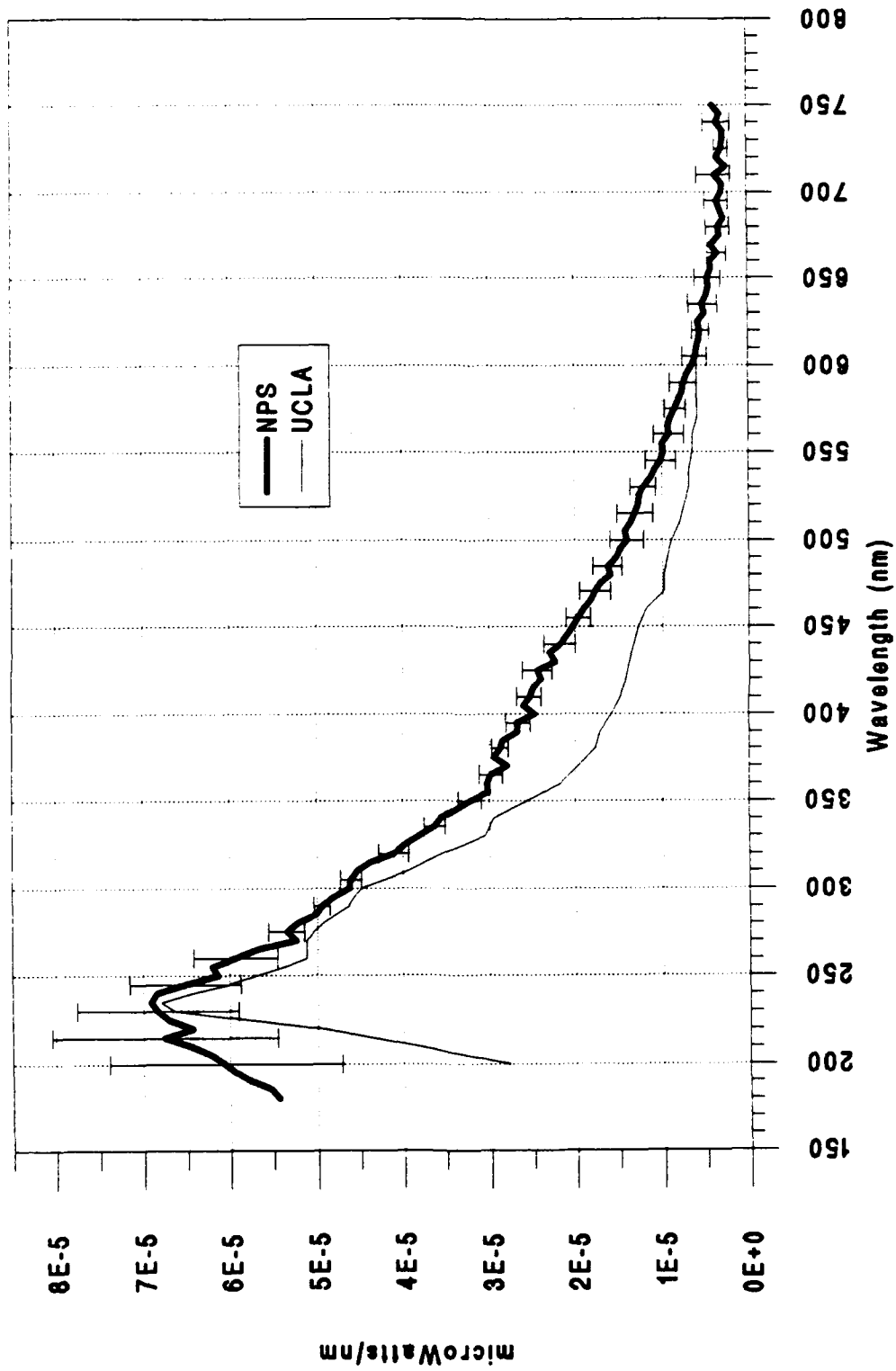


Figure 37 Comparison of NPS and UCLA SL Spectra in Water

absolute temperature of the blackbody. The energy distribution of a blackbody,  $M_\lambda$ , can be described by

$$M_\lambda = \frac{2\pi hc}{\lambda^5} \frac{1}{e^{\frac{hc}{\lambda kT}} - 1} \quad (2)$$

where  $h$  is Planck's constant,  $\lambda$  is the wavelength,  $c$  is the speed of light,  $k$  is Boltzmann's constant and  $T$  is the temperature of the blackbody. The units of  $M_\lambda$  are power per radiating area per wavelength interval. If Equation (2) is multiplied by the surface area of the radiating blackbody, the product becomes the total power radiated per wavelength interval by the blackbody.

It is recognized that the SL mechanism is probably a dynamic process without a constant temperature in time. Blackbody equilibrium may not necessarily be achieved. However, the spectra appear to have the gross characteristics of a blackbody. Fitting to a blackbody provides an average description of the spectra, regardless of any physical reality, and is a method of characterization.

The SL spectra were modeled by a blackbody radiation distribution to obtain an effective blackbody peak temperature and size for SL. A least squares fit to the SL spectra was performed with two parameters, radiating area  $A$ , and peak temperature  $T$ , with the equation

$$P = AM_\lambda = A \frac{2\pi hc}{\lambda^5} \frac{1}{e^{\frac{hc}{\lambda kT}} - 1} \quad (3)$$

where  $P$  is the power radiated per wavelength interval for a blackbody of area  $A$  and temperature  $T$ .

### 1. SL in Water Fit to a Blackbody Distribution

Equation (3) was modified with the appropriate constants to produce units for  $P$  of *picoWatts/nm*. Equation (3) was fit to Figure 30, the total power radiated from a single SL flash in water, to determine  $A$  and  $T$ . Figure 38 shows the resulting blackbody fit to Figure 30 and the fit parameters  $A$  and  $T$ .

### 2. SL in 25% Glycerin Fit to a Blackbody Distribution

Equation (3) was fit to Figure 32, the total power radiated from a single SL flash in a 25% glycerin solution. Figure 39 shows the resulting blackbody fit and the fit parameters  $A$  and  $T$ .

### 3. SL in 40% Glycerin Fit to a Blackbody Distribution

Equation (3) was fit to Figure 34, the total power radiated from a single SL flash in a 40% glycerin solution. Figure 40 shows the resulting blackbody fit and the fit parameters  $A$  and  $T$ . Although the forced fit to a blackbody distribution shows a higher temperature than for the 25% glycerin solution, Figure 40 illustrates that the distribution is not well fit.

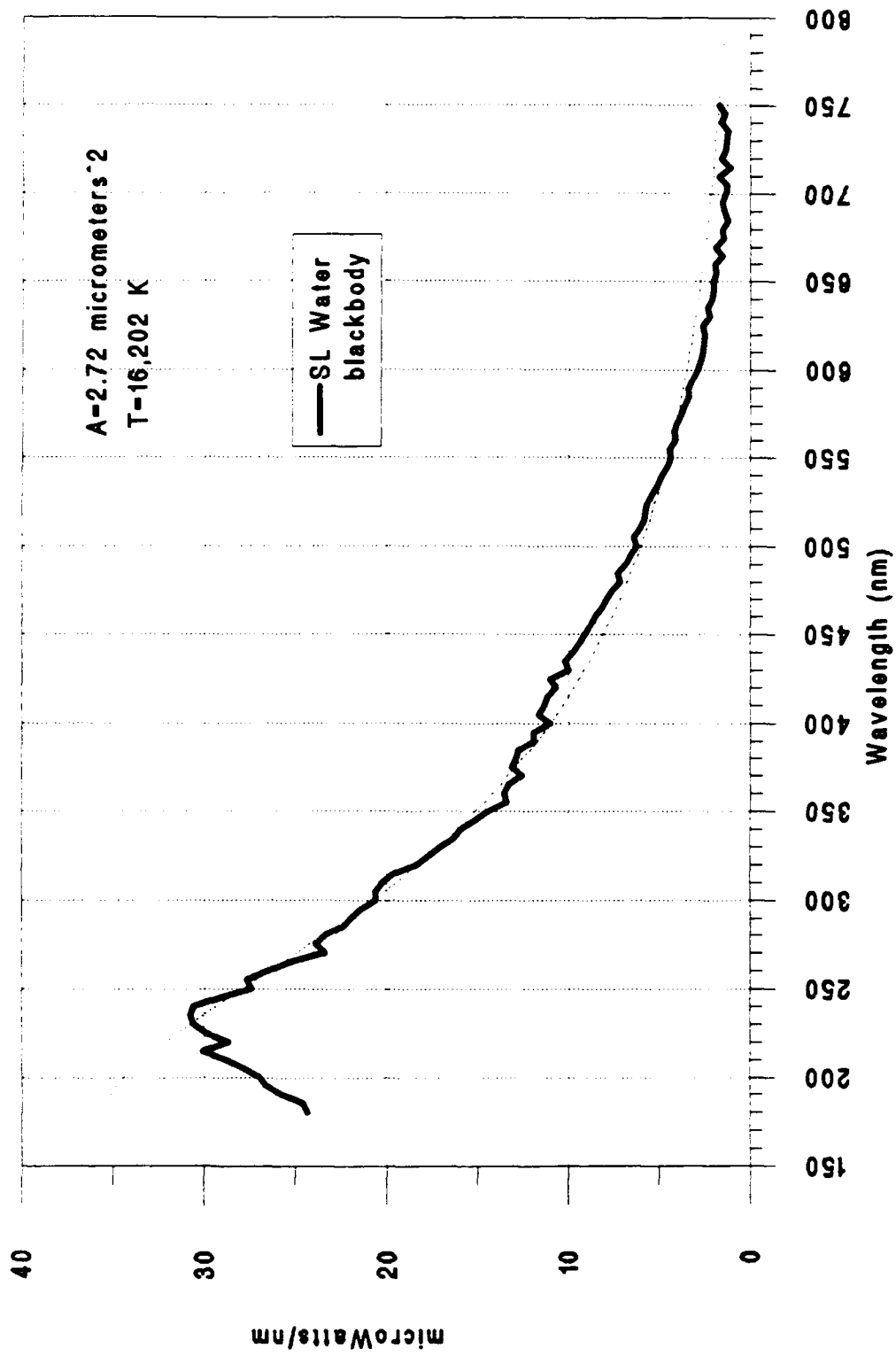


Figure 38 Blackbody Fit to SL in Water

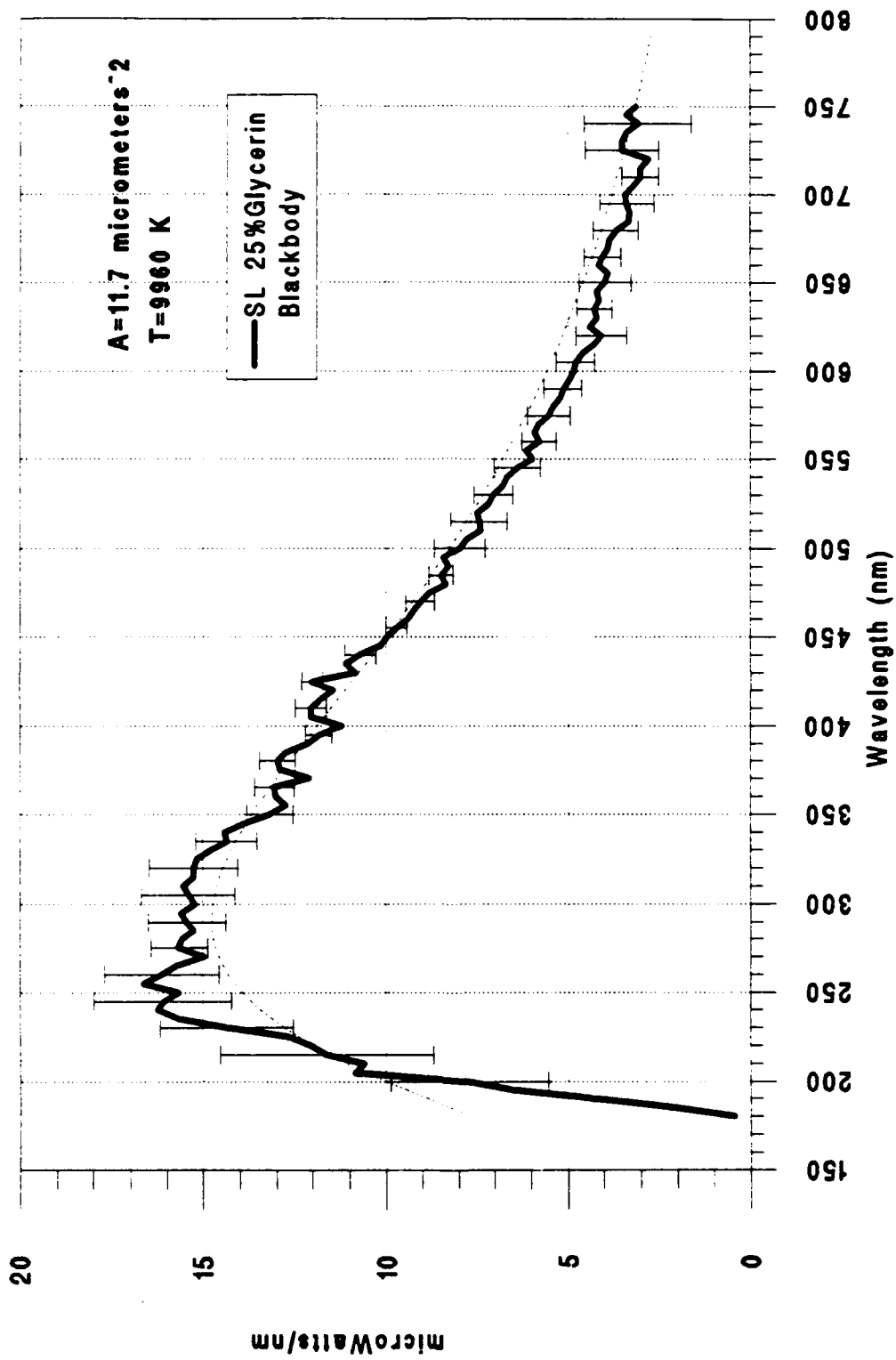


Figure 39 SL in 25% Glycerin Solution Fit to a Blackbody

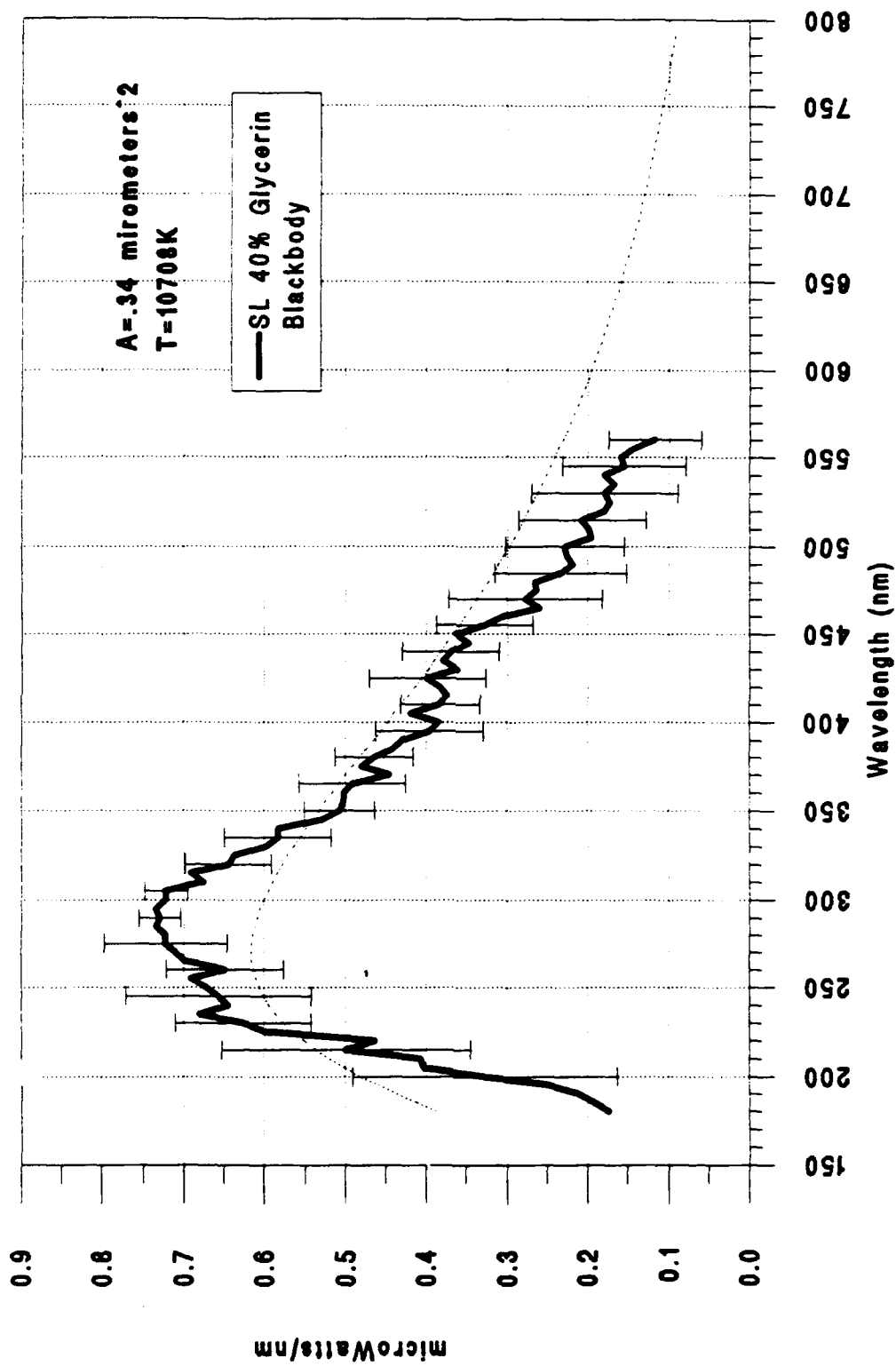


Figure 40 SL in 40% Glycerin Solution Fit to a Blackbody

#### 4. Comparison of Blackbody Fit Data

Table (2) summarizes the results of the SL data fit to Equation (3), the blackbody radiation distribution. The data indicates the effective temperature of SL in water is significantly greater than that of the glycerin solutions. All the solutions produce an effective blackbody radius in the sub-micrometer region.

TABLE (2)

Solution	BB Temp(K)	Area( $\mu\text{m}^2$ )	Radius( $\mu\text{m}$ )
water	16,202	2.72	.47
25% glycerin	9,960	11.70	.97
40% glycerin	10,708	0.34	.16

It is also interesting to note that the application of Wien's displacement law,

$$\lambda_{\text{max}}T = 2.898 \times 10^{-3} (m-K),$$

to the apparent observed peak wavelengths give effective blackbody temperatures of similar magnitudes to those listed in Table (2). Table (3) summarizes the results obtained from the application of Wien's displacement law. The effective temperature obtained for the 25% glycerin solution is identical for both methods.

TABLE (3)

Solution	$\lambda_{max}$	BB Temp (K)
Water	200	12,600
25% glycerin	260	9700
40% glycerin	300	8400

Current experimental measurements of the minimum bubble radius when SL is emitted indicate a radius of a few micrometers for SL in water [Ref. 8:p.2]. Therefore, the effective blackbody radius for water from Table (2) indicates that the radiating volume is about 1% of the measured minimum volume of the bubble. This result may indicate that the radiating medium for SL is much smaller than the physical gas-water interface.

**G. SL SPECTRA COMPARED TO CARLSON SPECTRA**

Another independent measurement of SL spectra was produced by Carlson using equipment at Lawrence Livermore National Laboratories. The spectra were produced with a spectrometer using a multichannel plate intensifier/CCD detector system. Carlson was able to record time elapsed exposures of the SL spectrum in 300 nm sections. He produced a spectrum for SL in water and a 25% glycerin solution in the wavelength range 400 nm to 650 nm.

Carlson also used the blackbody radiation distribution, Equation (3), to model his spectra as a blackbody. The blackbody effective temperatures and fit parameters provide a good comparison of the spectra presented in this work to spectra determined by Carlson. Table (4) summarizes the data comparison.

TABLE (4)

Spectra	Type	Temp (K)	Area ( $\mu\text{m}^2$ )	Rad. ( $\mu\text{m}$ )
Lewia	Water	16,202	2.72	.47
Carlson	Water	18,900	.41	.16
Lewia	25% glyc	9,960	11.70	.97
Carlson	25% glyc	14,300	1.3	.29

Both measurements indicate that the radiating temperatures are of similar magnitude. Apparent differences between this work and Carlson's work could originate from several sources. Among these sources are,

- Differences in the resonant frequency and amplitude.
- Differences in the geometry for photon capture. Carlson's work used a smaller fiber (100  $\mu\text{m}$  diam.) and a multichannel plate intensifier/CCD detector vs. a PMT.
- Differences in the time period of data collection. Carlson's work was based on a relatively short time period (30 s) entire spectrum exposure whereas this work used a much slower scanning method (10-15 min.).

- Differences in the absolute efficiency calibration. Different calibration sources were used in the two methods.

In addition, this work relied heavily on spectra at short wavelengths. Carlson's results were obtained from spectra between 400 nm and 650 nm. The general conclusions that require effective temperatures of over 10,000 K and an effective radiating volume smaller than the measured gas-water interface, hold true for both measurements.

## V. CONCLUSIONS

The spectrum of sonoluminescence was measured for water and water/glycerin mixtures. If the spectra are modeled by a blackbody radiation distribution, effective temperatures of 16,000 K and 10,000 K are obtained for water and 25% glycerin/75% water mixtures, respectively. Measurements of 40% water were also made but less reliably as the spectral intensity and bubble stability was not as well determined. The temperature fitted with the blackbody distribution is consistent with that obtained from the application of Wien's displacement law, although the wavelength for the maximum intensity is not well determined.

It was also determined that, if blackbody like radiation is the source of SL, the effective volume from which the radiation occurs is much smaller than the gas-water interface.

The general agreement with Carlson's work, which used a different measurement technique, and Putterman's water spectrum, gives confidence to the fact that the general SL spectrum features have been measured correctly. Because the mechanism for SL is not yet established, these measurements provide benchmarks which must be explained by any theory modeling SL.

The spectral measurement of SL was somewhat limited by the performance of the measurement equipment and the physical

characteristics of SL itself. SL spectra for various solutions were measured in the wavelength region 200 nm to 750 nm, and errors associated with the measurements were determined and reported.

SL spectra were found to be remarkably consistent for a given solution and highly repeatable, even with large variations in the driving force amplitude. The spectra, however, varied greatly depending on the solution content when compared with each other. All spectra emit the majority of their energy in the UV spectral region.

It was determined that, for solutions of water and glycerin, the greater the glycerin content the less intense SL becomes and the spectrum shifts toward longer wavelengths.

The SL spectra are hampered by uncertainties at the system wavelength limit of 200 nm. More suitable equipment, such as a grating centered at 200 nm or a more sensitive PMT, could significantly decrease the uncertainty in this region. A more certain measurement in this region would confirm or disprove the existence of a spectral peak in any of the measured spectra. However, the physical wavelength limit imposed by the liquid medium in which SL is produced places a hard lower boundary of about 185 nm on even the best spectral measurement of SL.

#### LIST OF REFERENCES

1. Frenzel and Schultes, *Z. physik. Chem.*, v. 27, 1934.
2. Chambers, L., *Journal of Chemical Physics*, v. 5, 1937.
3. Sehgal, C., Sutherland, R., Verrall, R., "Optical Spectra of Sonoluminescence from Transient and Stable Cavitation in Water Saturated with Various Gasses", *Journal of Physical Chemistry*, v. 84, 1980.
4. Gaitan, F., Crum, L., Church, C., Roy, R., "Sonoluminescence and Bubble Dynamics for a Single, Stable, Cavitation Bubble", *J. Acoust. Soc. Am.*, v. 91, 1992.
5. Barber, B., Hiller, R., Ariska, K., Fetterman, H., Putterman, S., "Resolving the Picosecond Characteristics of Synchronous Sonoluminescence", *J. Acoust. Soc. Am.*, v. 91, 1992.
6. Hiller, R., Putterman, S., Barber, B., "Spectrum of Synchronous Picosecond Sonoluminescence", *Phys. Rev. Lett.*, v. 69, 1992.
7. Carlson, J.T., *Visible Spectrum of Stable Sonoluminescence*, Master's Thesis, Naval Post Graduate School, Monterey, California, December 1992.
8. Barber, B., Putterman, S., "Light Scattering Measurements of the Repetitive Supersonic Implosion of a Sonoluminescent Bubble", Submitted to *Physical Review Letters*, September 1992.

### INITIAL DISTRIBUTION LIST

1. Defense Technical Information Center  
Cameron Station  
Alexandria, Virginia 22304-6145 2
2. Library, Code 52  
Naval Postgraduate School  
Monterey, California 93943-5002 2
3. Dr. Kai Woehler  
Physics Department, PH-WH  
Naval Postgraduate School  
Monterey, California 93943-5000 1
4. Dr. Xavier K. Maruyama  
Physics Department, PH-MX  
Naval Postgraduate School  
Monterey, California 93943-5000 10
5. Dr. Anthony A. Atchley  
Physics Department, PH-AY  
Naval Postgraduate School  
Monterey, California 93943-5000 2
6. Dr. Daniel Holland  
Physics Department, PH-HO  
Naval Postgraduate School  
Monterey, California 93943-5000 1
7. Dr. Felipe Gaitan  
Physics Department, PH-GN  
Naval Postgraduate School  
Monterey, California 93943-5000 1
8. Jerry Lentz  
Physics Department, PH  
Naval Postgraduate School  
Monterey, California 93943-5000 1
9. Dr. Mark E. Lowry  
University of California  
Lawrence Livermore National Laboratory  
P. O. Box 808, L-45  
Livermore, California 94550 1

10. Dr. Michael J. Moran  
 University of California  
 Lawrence Livermore National Laboratory  
 P. O. Box 808, L-41  
 Livermore, California 94550 1
  
11. Philip M. Armatis  
 University of California  
 Lawrence Livermore National Laboratory  
 P. O. Box 808, L-54  
 Livermore, California 94550 1
  
12. Darren R. Sweider  
 University of California  
 Lawrence Livermore National Laboratory  
 P. O. Box 808, L-130  
 Livermore, California 94550 1
  
13. Lt Joseph T. Carlson  
 c/o Carrie Rose  
 1141 Rte. 3 Read Road  
 Janesville, Wisconsin 53546 1
  
14. Lt Stephen D. Lewia  
 5 Merrifield Drive  
 Kennebunk, Maine 04043 2